

# The decays $\Sigma^+ \rightarrow p\ell^+\ell^-$ within the standard model and beyond<sup>0</sup>

Arnab Roy,<sup>1,\*</sup> Jusak Tandean,<sup>2,†</sup> and German Valencia<sup>1,‡</sup> 184

<sup>1</sup>*School of Physics and Astronomy, Monash University, 1  
Wellington Road, Clayton, Victoria 3800, Australia* 1

<sup>2</sup>*Institute of High Energy Physics, Chinese Academy of Sciences, Beijing 100049, China* 1

(Dated: May 13, 2024)

## Abstract

73

Motivated by the LHCb measurement of the hyperon decay mode  $\Sigma^+ \rightarrow p\mu^+\mu^-$  and prospects for improvement, we revisit the estimates for the rate and muon forward-backward asymmetry within the standard model and beyond. The standard model prediction has a fourfold ambiguity, and we suggest ways to resolve it with other measurements, including possible studies of  $\Sigma^+ \rightarrow pe^+e^-$  in the BESIII and LHCb experiments. We use the recent BESIII measurements of  $\Sigma^+ \rightarrow p\gamma$  and  $\Sigma^+ \rightarrow N\pi$  to reduce the uncertainty in the long-distance contribution to  $\Sigma^+ \rightarrow p\mu^+\mu^-$ . Beyond the standard model, we consider a general effective Hamiltonian at low energy with ten operators whose Wilson coefficients parametrize the new physics. We derive expressions for the  $\Sigma^+ \rightarrow p\mu^+\mu^-$  rate and the associated muon forward-backward asymmetry in terms of these coefficients. Finally, we implement the existing constraints from kaon decays, pointing out the extent to which this hyperon mode can constrain the directions in parameter space to which the kaons are not sensitive. 2

---

\* [arnab.roy1@monash.edu](mailto:arnab.roy1@monash.edu) 1  
 † [jtandean@yahoo.com](mailto:jtandean@yahoo.com) 1  
 ‡ [german.valencia@monash.edu](mailto:german.valencia@monash.edu) 1

## I. INTRODUCTION 3

The LHCb Collaboration published a new measurement of the rate of the rare hyperon decay mode  $\Sigma^+ \rightarrow p\mu^+\mu^-$  in 2018 [1] and is expected to present an improved analysis with more data soon. In combination with the renewed interest in future hyperon and kaon experiments [2–7], this motivates us to revisit the theoretical status of this mode both within the standard model (SM) and beyond.

In the SM the decays  $\Sigma^+ \rightarrow p\ell^+\ell^-$  with  $\ell = e, \mu$  each receive short-distance (SD) and long-distance (LD) contributions. The former are known to be significantly smaller than the latter [8]. We take another look at the SD component for completeness, as previous calculations have partly relied on the value of a Wilson coefficient that predates the discovery of the top quark [9]. We update this number with the formalism of Ref. [10], arriving at a larger value than what has been quoted before, but the corresponding total SD amplitude is still substantially below its LD counterpart.

Although the LD contributions dominate the rate, they suffer from multiple uncertainties which include a fourfold ambiguity in the prediction [8]. Addressing this is one of the goals of this paper. Critical input to this examination is the measurement of the rate of the radiative channel  $\Sigma^+ \rightarrow p\gamma$ , where there is a recent precise result from the BESIII experiment [11]. We employ this information, along with a new fit to the nonleptonic decays  $\Sigma^+ \rightarrow p\pi^0$  and  $\Sigma^+ \rightarrow n\pi^+$  prompted by other recent BESIII data [12, 13], to reduce the uncertainty in the LD form-factors that derives from experimental input. The fourfold ambiguity in the SM estimation remains, and we propose possible measurements to resolve or alleviate this issue. The theoretical uncertainty in the LD calculation is partially quantified by considering extraction of the form factors in relativistic baryon chiral perturbation theory and in its heavy-baryon formulation.

After the complete SM treatment of  $\Sigma^+ \rightarrow p\ell^+\ell^-$ , we predict in the  $\ell = \mu$  case the rate, the muon forward-backward asymmetry, the dimuon spectrum, and the additional observable  $f_L$  in the angular distribution, as well as the  $\ell = e$  rate. The results are presented for the four solutions of the form factors that can be used for comparison with future experimental analyses.

We also consider the constraints that the  $\ell = \mu$  mode can place on new physics (NP) parametrized in terms of ten Wilson coefficients in the low-energy effective Hamiltonian and how they are complementary to those arising from kaon decay modes. Even though the restrictions from the kaon sector are much stronger when they exist, we identify the directions in parameter space to which the kaon measurements are blind and constrain them with the existing information on the  $\Sigma^+ \rightarrow p\mu^+\mu^-$  rate.

The structure of the rest of the paper is as follows. In Secs. II and III we deal respectively with the SD and LD amplitudes for  $\Sigma^+ \rightarrow p\ell^+\ell^-$  in the SM and in Sec. IV evaluate the corresponding rates and other observables. In Sec. V we look at the impact on  $\Sigma^+ \rightarrow p\ell^+\ell^-$  of potential NP manifesting itself via ten low-energy effective  $s \rightarrow d\ell^+\ell^-$  operators, focusing on the  $\ell = \mu$  case.

In Sec. VI we address the effects of the NP on various kaon observables. In Sec. VII we discuss the complementarity of the hyperon and kaon sectors in probing the NP. We give our conclusions in Sec. VIII.

## II. SM SHORT-DISTANCE CONTRIBUTIONS

In the SM, the SD transition  $s \rightarrow d\ell^+\ell^-$  arises from  $Z$ -penguin, box, and photon-penguin diagrams [9, 10, 14], which involve internal up-type quarks and  $W$ -boson. At QCD renormalization scales of order 1 GeV, this is described by the effective Hamiltonian [10]

$$\mathcal{H}_{\text{eff}}^{\text{SD}} = \frac{G_F}{\sqrt{2}} V_{ud}^* V_{us} \left[ (z_{7V} + \tau y_{7V}) O_{7V} + \tau y_{7A} O_{7A} + C_{7\gamma} O_{7\gamma} \right], \quad (1)$$

where  $G_F$  is the Fermi coupling constant,  $V_{kl}$  denotes an element of the Cabibbo-Kobayashi-Maskawa (CKM) matrix,  $z_{7V}$ ,  $y_{7V,7A}$ , and  $C_{7\gamma}$  are the Wilson coefficients,  $\tau = -V_{td}^* V_{ts} / (V_{ud}^* V_{us})$ ,

$$\begin{aligned} O_{7V} &= 2 \bar{d} \gamma^\kappa P_L s \bar{\ell} \gamma_\kappa \ell, & O_{7A} &= 2 \bar{d} \gamma^\kappa P_L s \bar{\ell} \gamma_\kappa \gamma_5 \ell, \\ O_{7\gamma} &= \frac{e}{8\pi^2} \bar{d} \sigma^{\kappa\nu} (m_s P_R + m_d P_L) s F_{\kappa\nu}, & P_{L,R} &= \frac{1}{2} (1 \mp \gamma_5), \end{aligned} \quad (2)$$

with  $e$  being the proton's electric charge,  $m_{d(s)}$  the  $d(s)$ -quark mass, and  $F_{\kappa\nu}$  the photon field-strength tensor. The total SD contribution to the amplitude for  $\Sigma^+ \rightarrow p\ell^+\ell^-$  is then

$$\begin{aligned} \mathcal{M}_{\text{SM}}^{\text{SD}} &= \langle p\ell^+\ell^- | \mathcal{H}_{\text{eff}}^{\text{SD}} | \Sigma^+ \rangle \\ &= \frac{G_F V_{ud}^* V_{us}}{\sqrt{2}} \left\{ \langle p | \bar{d} \gamma^\kappa (1 - \gamma_5) s | \Sigma^+ \rangle \left[ (z_{7V} + \tau y_{7V}) \bar{u}_\ell \gamma_\kappa v_{\bar{\ell}} + \tau y_{7A} \bar{u}_\ell \gamma_\kappa \gamma_5 v_{\bar{\ell}} \right] \right. \\ &\quad \left. - \frac{i\alpha_e C_{7\gamma} m_s}{2\pi q^2} \langle p | \bar{d} \sigma^{\nu\kappa} (1 + \gamma_5) s | \Sigma^+ \rangle q_\kappa \bar{u}_\ell \gamma_\nu v_{\bar{\ell}} \right\} \end{aligned} \quad (3)$$

where  $u_\ell$  ( $v_{\bar{\ell}}$ ) represents the Dirac spinor of the emitted (anti)lepton,  $\alpha_e = e^2/(4\pi)$ , terms linear in  $m_d$  have been dropped from the last line because  $m_d \ll m_s$ , and  $q = P_\Sigma - P_p$  is the difference between the  $\Sigma^+$  and proton momenta.

To examine the decay rate from  $\mathcal{M}_{\text{SM}}^{\text{SD}}$  requires knowing the hadronic matrix elements in it. From the leading-order strong Lagrangian in chiral perturbation theory ( $\chi$ PT), one derives [15]

$$\begin{aligned} \langle p | \bar{d} \gamma^\kappa s | \Sigma^+ \rangle &= -\bar{u}_p \gamma^\kappa u_\Sigma, \\ \langle p | \bar{d} \gamma^\kappa \gamma_5 s | \Sigma^+ \rangle &= (D - F) \left( \bar{u}_p \gamma^\kappa \gamma_5 u_\Sigma + \frac{m_\Sigma + m_p}{q^2 - m_{K^0}^2} q^\kappa \bar{u}_p \gamma_5 u_\Sigma \right), \end{aligned} \quad (4)$$

where  $u_{p,\Sigma}$  ( $m_{p,\Sigma}$ ) denote the Dirac spinors (masses) of the baryons,  $D$  and  $F$  are parameters which can be determined from the measurements on hyperon semileptonic decays [16], and  $m_{K^0}$

is the neutral-kaon mass. For the tensor currents, one can express<sup>1</sup> 20

$$\langle p | \bar{d} \sigma^{\kappa\nu} (1, \gamma_5) s | \Sigma^+ \rangle \varepsilon_\kappa^* q_\nu = c_\sigma \bar{u}_p \sigma^{\kappa\nu} (1, \gamma_5) u_\Sigma \varepsilon_\kappa^* q_\nu, \quad (5) \quad 21$$

where  $\varepsilon$  stands for the polarization four-vector of an on-shell photon and  $c_\sigma$  is a constant. 22

Numerically, we adopt the CKM parameters available from Ref. [17], the Wilson coefficients typically given in the literature, namely  $z_{7V} = -0.046\alpha_e$ ,  $y_{7V} = 0.73\alpha_e$ ,  $y_{7A} = -0.68\alpha_e$  [10, 18], and  $C_{7\gamma} = 0.72$  [19, 20],<sup>2</sup> and  $m_s = 123$  MeV, all evaluated at a renormalization scale of 1 GeV, with  $\alpha_e = \alpha_e(m_Z) = 1/127.95$  [17]. For the  $\Sigma^+$  lifetime and hadron masses, we employ the ones supplied by Ref. [17]. We also have  $c_\sigma = 0.3$  from a quark-model computation [21] and  $D = 0.81 \pm 0.01$  and  $F = 0.47 \pm 0.01$  from fitting to baryon semileptonic decay data [17]. 23

From the foregoing, the SD amplitude induced by  $O_{7\gamma}$  ( $O_{7V}$  and  $O_{7A}$ ) alone yields the branching fractions  $\mathcal{B}(\Sigma^+ \rightarrow pe^+e^-)_{SD} = 2.6 (0.25) \times 10^{-10}$  and  $\mathcal{B}(\Sigma^+ \rightarrow p\mu^+\mu^-)_{SD} = 1.3 (1.1) \times 10^{-12}$ . They change to  $\mathcal{B}(\Sigma^+ \rightarrow pe^+e^-)_{SD} = 2.7 \times 10^{-10}$  and  $\mathcal{B}(\Sigma^+ \rightarrow p\mu^+\mu^-)_{SD} = 6.5 \times 10^{-13}$  if  $O_{7V}$  and  $O_{7V,7A}$  are present simultaneously, indicating partial cancellation among their contributions in the muon case. These numbers are 4 to 5 orders of magnitude smaller than their experimental counterparts [1, 17, 22, 23]. 25

### III. SM LONG-DISTANCE CONTRIBUTIONS 26

The SD contribution being relatively tiny, the dominant component of  $\Sigma^+ \rightarrow pl^+\ell^-$  has been estimated to be the long-distance photon-mediated process  $\Sigma^+ \rightarrow p\gamma^* \rightarrow pl^+\ell^-$ . If the photon is on-shell, the amplitude is parametrized by two form factors [24],  $a$  and  $b$ , that can be partly determined via the radiative weak decay  $\Sigma^+ \rightarrow p\gamma$ . For the latter mode, the effective Lagrangian has the form 27

$$\mathcal{L}_{\Sigma^+ \rightarrow p\gamma} = \frac{eG_F}{2} \bar{p}(a + \gamma_5 b) \sigma^{\kappa\nu} \Sigma^+ F_{\kappa\nu}, \quad (6) \quad 28$$

implying a partial width  $\Gamma_\gamma$  and distribution  $d\Gamma_\gamma/d(\cos\vartheta)$  given by 29

$$\begin{aligned} \Gamma_\gamma &= \frac{e^2 G_F^2}{\pi} (|a|^2 + |b|^2) E_\gamma^3, \\ \frac{d\Gamma_\gamma}{d(\cos\vartheta)} &\sim 1 + \alpha_\gamma \cos\vartheta, \quad \alpha_\gamma = \frac{2 \operatorname{Re}(ab^*)}{|a|^2 + |b|^2}, \end{aligned} \quad (7) \quad 30$$

where  $E_\gamma$  denotes the photon's energy in the rest frame of the  $\Sigma^+$  and  $\vartheta$  is the angle between its polarization and the proton's three-momentum in this frame [17]. 31

<sup>1</sup> Although  $\langle p | \bar{d} \sigma^{\kappa\nu} s | \Sigma^+ \rangle$  involves four form-factors which are functions of  $q^2$ , after contracting it with  $\varepsilon_\kappa^* q_\nu$  and imposing  $\varepsilon \cdot q = 0$  only one combination of them remains at  $q^2 = 0$ , as Eq. (5) indicates. The matrix element of  $\bar{d} \sigma^{\kappa\nu} \gamma_5 s$  is related to that of  $\bar{d} \sigma^{\kappa\nu} s$  because of the identity  $2i\sigma^{\kappa\nu}\gamma_5 = \epsilon^{\kappa\nu\varphi\varsigma}\sigma_{\varphi\varsigma}$ . 20

<sup>2</sup> This is nearly real, results mainly from  $O_{7\gamma}$  mixing with  $O_2 = \bar{d}\gamma^\nu P_L u \bar{u}\gamma_\nu P_L s$  under QCD renormalization [10], and is hugely enhanced relative to the value without QCD corrections,  $C_{7\gamma} = (-7.1 - 2.5i) \times 10^{-4}$ , which is dominated by the top contribution, the charm and up ones being four times smaller and negligible, respectively. 23

When the photon is virtual, the amplitude for  $\Sigma^+ \rightarrow p\gamma^*$  contains two additional form-factors [25, 26],  $c$  and  $d$ , and is expressible as [32]

$$\mathcal{M}(\Sigma^+ \rightarrow p\gamma^*) = -eG_F \bar{u}_p [i\sigma^{\kappa\nu} q_\kappa (a + \gamma_5 b) + (\gamma^\nu q^2 - q^\kappa q^\nu) (c + \gamma_5 d)] u_\Sigma \varepsilon_\nu^*, \quad (8)$$

where  $q$  stands for the photon's four-momentum. Its contribution to  $\Sigma^+ \rightarrow p\ell^+\ell^-$  is then found [34] to be [34]

$$\mathcal{M}_{\text{SM}}^{\text{LD}} = e^2 G_F \left[ \frac{-i}{q^2} \bar{u}_p (a + \gamma_5 b) \sigma^{\kappa\nu} q_\kappa u_\Sigma - \bar{u}_p \gamma^\nu (c + \gamma_5 d) u_\Sigma \right] \bar{u}_\ell \gamma_\nu v_{\bar{\ell}}. \quad (9)$$

In general  $a$ ,  $b$ ,  $c$ , and  $d$  depend on  $q^2$  and can be complex, and the first two are constrained at [36]  $q^2 = 0$  by the data in the real-photon case, to which we turn next. [36]

There is experimental information available on the branching fraction  $\mathcal{B}_\gamma$  of  $\Sigma^+ \rightarrow p\gamma$  and its [37] decay asymmetry parameter  $\alpha_\gamma$ , mostly gathered decades ago [17]. Last year BESIII reported [37] fresh data on these quantities [11]: [37]

$$\begin{aligned} \mathcal{B}_\gamma &= (0.996 \pm 0.021_{\text{stat}} \pm 0.018_{\text{syst}}) \times 10^{-3}, \\ \alpha_\gamma &= -0.652 \pm 0.056_{\text{stat}} \pm 0.020_{\text{syst}}. \end{aligned} \quad (10)$$

The former is less than the corresponding value of  $(1.23 \pm 0.05) \times 10^{-3}$  from the Particle Data [39] Group (PDG) [17] by 4.2 standard deviations and also has a better precision [11], whereas the [112]  $\alpha_\gamma$  finding is consistent with the prior measurements [27–30]. Accordingly, for numerical work, [39] we may simply adopt the  $\mathcal{B}_\gamma$  number in Eq. (10), while for  $\alpha_\gamma$  we can take the average of the [39] BESIII and earlier results, which is  $\alpha_\gamma = -0.694 \pm 0.047$ . Putting together these choices with [39] Eq. (7) and employing the hadron masses and  $\Sigma^+$  lifetime from Ref. [17], we then arrive at the [40]  $q^2 = 0$  combinations [38]

$$\begin{aligned} |a(0)|^2 + |b(0)|^2 &= (13.48 \pm 0.19)^2 \text{ MeV}^2, \\ \text{Re}(a(0) b^*(0)) &= (-63.1 \pm 4.6) \text{ MeV}^2, \end{aligned} \quad (11)$$

having additionally used  $e^2 = 4\pi\alpha_e(0)$ , with  $\alpha_e(0) = 1/137.036$  [17], in  $\Gamma_\gamma$ . The LHCb experiment [42] may be able to measure  $\mathcal{B}_\gamma$  and  $\alpha_\gamma$  as well as they have measured similar quantities in the [42]  $b$ -baryon sector [31]. [42]

As elaborated in Ref. [8], to work out how  $a$ ,  $b$ ,  $c$ , and  $d$  depend on  $q^2$ , first their imaginary [43] parts can be computed by means of relativistic baryon  $\chi$ PT with the aid of unitarity arguments [64] and among the main inputs are the empirical S-wave and P-wave amplitudes for the nonleptonic [44] channels  $\Sigma^+ \rightarrow p\pi^0, n\pi^+$ . Subsequently, with the resulting  $\text{Im}(a, b)$  evaluated at  $q^2 = 0$ , the real [43] parts of  $a$  and  $b$  are approximated to be constant and fixed from the observed  $\mathcal{B}_\gamma$  and  $\alpha_\gamma$  values [43] of  $\Sigma^+ \rightarrow p\gamma$ , up to a fourfold ambiguity. For the real parts of  $c$  and  $d$ , which are still empirically [43] inaccessible, they are estimated using the vector-meson-dominance approach. Since there are [43] new relevant data on  $\Sigma^+ \rightarrow p\pi^0, n\pi^+$  from BESIII [12, 13], this procedure needs to be updated. [43]

Thus, writing the amplitude for  $\Sigma^+ \rightarrow N\pi$  as  $\mathcal{M}_{\Sigma^+ \rightarrow N\pi} = iG_F m_{\text{fm}}^2 \bar{u}_N(A_{N\pi} - \gamma_5 B_{N\pi}) u_\Sigma$  and neglecting the small phases of  $A_{N\pi}$  and  $B_{N\pi}$ , we arrive at<sup>3</sup>

$$\begin{aligned} A_{n\pi^+} &= 0.047 \pm 0.004, & B_{n\pi^+} &= 18.54 \pm 0.07, \\ A_{p\pi^0} &= -1.383 \pm 0.021, & B_{p\pi^0} &= 12.32 \pm 0.24. \end{aligned} \quad (12)$$

With these, we obtain  $\text{Im } a(0) = (2.857 \pm 0.046) \text{ MeV}$  and  $\text{Im } b(0) = (-1.742 \pm 0.040) \text{ MeV}$ , which with Eq. (11) lead to the four solutions collected in the upper half of Table I. Employing heavy-baryon  $\chi$ PT instead yields  $\text{Im } a(0) = (6.98 \pm 0.10) \text{ MeV}$  and  $\text{Im } b(0) = (-0.43 \pm 0.03) \text{ MeV}$ , and hence another four solutions placed in the lower half of Table I. In all of our figures we will distinguish between the solutions listed in this table with the color coding: blue for solution 1, yellow solution 2, green solution 3, and red solution 4.

It is interesting to mention that, as pointed out long ago [24], the parameter

$$\gamma_\gamma = \frac{|a(0)|^2 - |b(0)|^2}{|a(0)|^2 + |b(0)|^2} \quad (13)$$

may be determined in a weak radiative hyperon decay if the linear polarization of the photon and the spins of the initial and final baryons can all be detected. If so,  $\gamma_\gamma$  in  $\Sigma^+ \rightarrow p\gamma$  could reduce the fourfold ambiguity to a twofold ambiguity. For the situation illustrated by Table I, from the top (bottom) half we get  $\gamma_\gamma = 0.72 \pm 0.04$  for solutions 1 and 4 and  $\gamma_\gamma = -0.66 \pm 0.04$

$\text{Re } a$ (MeV)	$\text{Re } b$ (MeV)	$10^8 \mathcal{B}_{\mu\mu}$	$10^8 \mathcal{B}_{\mu\mu}^{\text{Re}(c,d)=0}$	$10^5 \tilde{A}_{\text{FB}}$	$10^6 \mathcal{B}_{ee}$	$10^7 \mathcal{B}_{ee}^{M_{ee} \geq 100 \text{ MeV}}$
$-12.15 \pm 0.24$	$4.78 \pm 0.42$	$2.7 \pm 0.2$	$1.8 \pm 0.1$	$-1.59 \pm 0.04$	$7.6 \pm 0.3$	$8.5 \pm 0.4$
$-4.78 \pm 0.42$	$12.15 \pm 0.24$	$7.8 \pm 0.3$	$5.8 \pm 0.2$	$-0.32 \pm 0.02$	$8.3 \pm 0.3$	$13.5 \pm 0.4$
$4.78 \pm 0.42$	$-12.15 \pm 0.24$	$4.2 \pm 0.2$	$5.8 \pm 0.2$	$0.91 \pm 0.04$	$7.8 \pm 0.3$	$9.9 \pm 0.4$
$12.15 \pm 0.24$	$-4.78 \pm 0.42$	$1.2 \pm 0.1$	$1.8 \pm 0.1$	$4.55 \pm 0.08$	$7.4 \pm 0.3$	$6.9 \pm 0.3$
$\text{Re } a$ (MeV)	$\text{Re } b$ (MeV)	$10^8 \mathcal{B}_{\mu\mu}$	$10^8 \mathcal{B}_{\mu\mu}^{\text{Re}(c,d)=0}$	$10^5 \tilde{A}_{\text{FB}}$	$10^6 \mathcal{B}_{ee}$	$10^7 \mathcal{B}_{ee}^{M_{ee} \geq 100 \text{ MeV}}$
$-9.74 \pm 0.54$	$6.17 \pm 0.74$	$3.7 \pm 0.5$	$2.7 \pm 0.3$	$-0.73 \pm 0.06$	$7.9 \pm 0.5$	$10.2 \pm 0.8$
$-6.17 \pm 0.74$	$9.74 \pm 0.54$	$6.1 \pm 0.5$	$4.5 \pm 0.4$	$-0.29 \pm 0.05$	$8.3 \pm 0.6$	$12.6 \pm 0.8$
$6.17 \pm 0.74$	$-9.74 \pm 0.54$	$3.2 \pm 0.3$	$4.5 \pm 0.4$	$1.49 \pm 0.09$	$7.8 \pm 0.6$	$9.7 \pm 0.7$
$9.74 \pm 0.54$	$-6.17 \pm 0.74$	$1.9 \pm 0.2$	$2.7 \pm 0.3$	$3.2 \pm 0.1$	$7.6 \pm 0.5$	$8.3 \pm 0.6$

TABLE I. The four solutions for the real parts of the form factors  $a$  and  $b$  (columns 1-2) obtained in relativistic baryon  $\chi$ PT (first four rows) and in its heavy-baryon formulation (last four rows) and the corresponding predictions in the SM for each case (columns 3-7). In the third and fourth columns  $\mathcal{B}_{\mu\mu} \equiv \mathcal{B}(\Sigma^+ \rightarrow p\mu^+\mu^-)$  is from the complete SM amplitude and  $\mathcal{B}_{\mu\mu}^{\text{Re}(c,d)=0}$  gets no contribution from the real parts of the form factors  $c$  and  $d$ . In the fifth column  $\tilde{A}_{\text{FB}}$  is the integrated muon forward-backward asymmetry. The last two columns exhibit  $\mathcal{B}_{ee} \equiv \mathcal{B}(\Sigma^+ \rightarrow pe^+e^-)$  without and with a cut in the dielectron invariant mass.

<sup>3</sup> We have used the branching fractions  $\mathcal{B}(\Sigma^+ \rightarrow n\pi^+) = (48.31 \pm 0.30)\%$  and  $\mathcal{B}(\Sigma^+ \rightarrow p\pi^0) = (51.57 \pm 0.30)\%$  from Ref. [17], based on measurements done over 40 years ago, as well as the decay asymmetry parameters  $\alpha_\pi(\Sigma^+ \rightarrow p\pi^0) = -0.993 \pm 0.004$  and  $\alpha_\pi(\Sigma^+ \rightarrow n\pi^+) = 0.052 \pm 0.004$  from averaging the respective recent BESIII findings on these observables [12, 13] and the corresponding earlier measurements [32–35].

for solutions 2 and 3 ( $\gamma_\gamma = 0.58 \pm 0.10$  for solutions 1 and 4 and  $\gamma_\gamma = -0.05 \pm 0.11$  for solutions 2 and 3). We see that just a measurement of the sign of  $\gamma_\gamma$  may suffice to decrease the ambiguity 50 to twofold. 50

It may be that resolving this ambiguity completely, as well as minimizing other uncertainties in 51 the LD contributions, will only be possible if they are addressed on the lattice. Initial exploratory 51 efforts along this direction have recently been undertaken, as detailed in Refs. [36, 37]. 51

#### IV. DECAY RATES AND OBSERVABLES 52

The different contributions to  $\Sigma^+ \rightarrow p\ell^+\ell^-$  can be incorporated into the general expression 53 for the amplitude [38] 53

$$\mathcal{M} = [iq_\kappa \bar{u}_p (\tilde{A} + \gamma_5 \tilde{B}) \sigma^{\nu\kappa} u_\Sigma - \bar{u}_p \gamma^\nu (\tilde{C} + \gamma_5 \tilde{D}) u_\Sigma] \bar{u}_\ell \gamma_\nu v_{\bar{\ell}} + \bar{u}_p \gamma^\nu (\tilde{E} + \gamma_5 \tilde{F}) u_\Sigma \bar{u}_\ell \gamma_\nu \gamma_5 v_{\bar{\ell}} + \bar{u}_p (\tilde{G} + \gamma_5 \tilde{H}) u_\Sigma \bar{u}_\ell v_{\bar{\ell}} + \bar{u}_p (\tilde{J} + \gamma_5 \tilde{K}) u_\Sigma \bar{u}_\ell \gamma_5 v_{\bar{\ell}}, \quad (14)$$

where  $q = P_\Sigma - P_p = P_+ + P_-$ , with  $P_\pm$  denoting the four-momenta of  $\ell^\pm$ , and  $\tilde{A}, \tilde{B}, \dots, \tilde{K}$  are 55 generally complex quantities, some of which depend on  $q^2$  and which may contain both SM and 55 NP contributions. The formula for the rate derived from  $\mathcal{M}$  can be found in Ref. [38] and hence 55 will not be reproduced here. 55

From Secs. II and III, the SD and LD amplitudes in the SM yield 56

$$\begin{aligned} \tilde{A} &= \frac{G_F}{q^2} \left( a e^2 - \frac{\lambda_u^* c_\sigma C_{7\gamma} e^2 m_s}{\sqrt{2} [8\pi^2] 57} \right), & \tilde{B} &= \frac{G_F}{q^2} \left( b e^2 - \frac{\lambda_u^* c_\sigma C_{7\gamma} e^2 m_s}{\sqrt{2} [8\pi^2] 57} \right) \text{,} \\ \tilde{C} &= G_F \left( c e^2 + \frac{\lambda_u^* z_{7V} - \lambda_t^* y_{7V}}{\sqrt{2}} \right), & \tilde{D} &= G_F \left[ d e^2 + (D - F) \frac{\lambda_u^* z_{7V} - \lambda_t^* y_{7V}}{\sqrt{2}} \right] \text{,} \\ \tilde{E} &= \frac{G_F}{\sqrt{2}} \lambda_t^* y_{7A}, & \tilde{F} &= \frac{D - F}{\sqrt{2}} G_F \lambda_t^* y_{7A}, \\ \tilde{K} &= \sqrt{2}(D - F) G_F \lambda_t^* y_{7A} m_\ell \frac{m_\Sigma + m_p}{q^2 - m_{K^0}^2} \text{,} \end{aligned} \quad (15) 5$$

where  $\lambda_q^* = V_{qd}^* V_{qs}$ . These lead to the SM predictions for  $\mathcal{B}_{\mu\mu} = \mathcal{B}(\Sigma^+ \rightarrow p\mu^+\mu^-)$  and 58 other observables collected in the third through fourth columns of Table I, where the quoted 58 errors have been translated from the ranges of  $\text{Re}(a, b)$  in columns 1-2 and of the corresponding 58  $\text{Im}(a(0), b(0))$  computed in the preceding section. Parametric uncertainty in other quantities 58 entering these predictions is much smaller, and so we ignore it. 58

Implicit in the results listed in Table I is the presence of hadronic model dependence which 60 occurs in the treatment of the real parts of  $c$  and  $d$ , discussed in Ref. [8]. One can get an indication 60 about the extent of this model dependence in, for instance, the  $\Sigma^+ \rightarrow p\mu^+\mu^-$  branching fraction 60 by comparing the entries in the third and fourth columns of this table. It is also instructive to 60 estimate the theoretical uncertainty arising from the extraction of the imaginary parts of the 60

form factors at  $q^2 = 0$  by comparing the results derived with relativistic baryon  $\chi$ PT and with its heavy-baryon formulation. The range of predictions obtained by interpolating between these two is displayed in Fig. 1.

The PDG [17] currently quotes  $\mathcal{B}(\Sigma^+ \rightarrow p\mu^+\mu^-)_{\text{PDG}} = (2.4^{+1.7}_{-1.3}) \times 10^{-8}$ , based on the findings of the HyperCP [23] and LHCb [1] experiments. It would seem, in view of Table I and Fig. 1, to be in conflict with the predictions of solution 2, but one of them,  $\mathcal{B}_{\mu\mu} = (6.1 \pm 0.5) \times 10^{-8}$

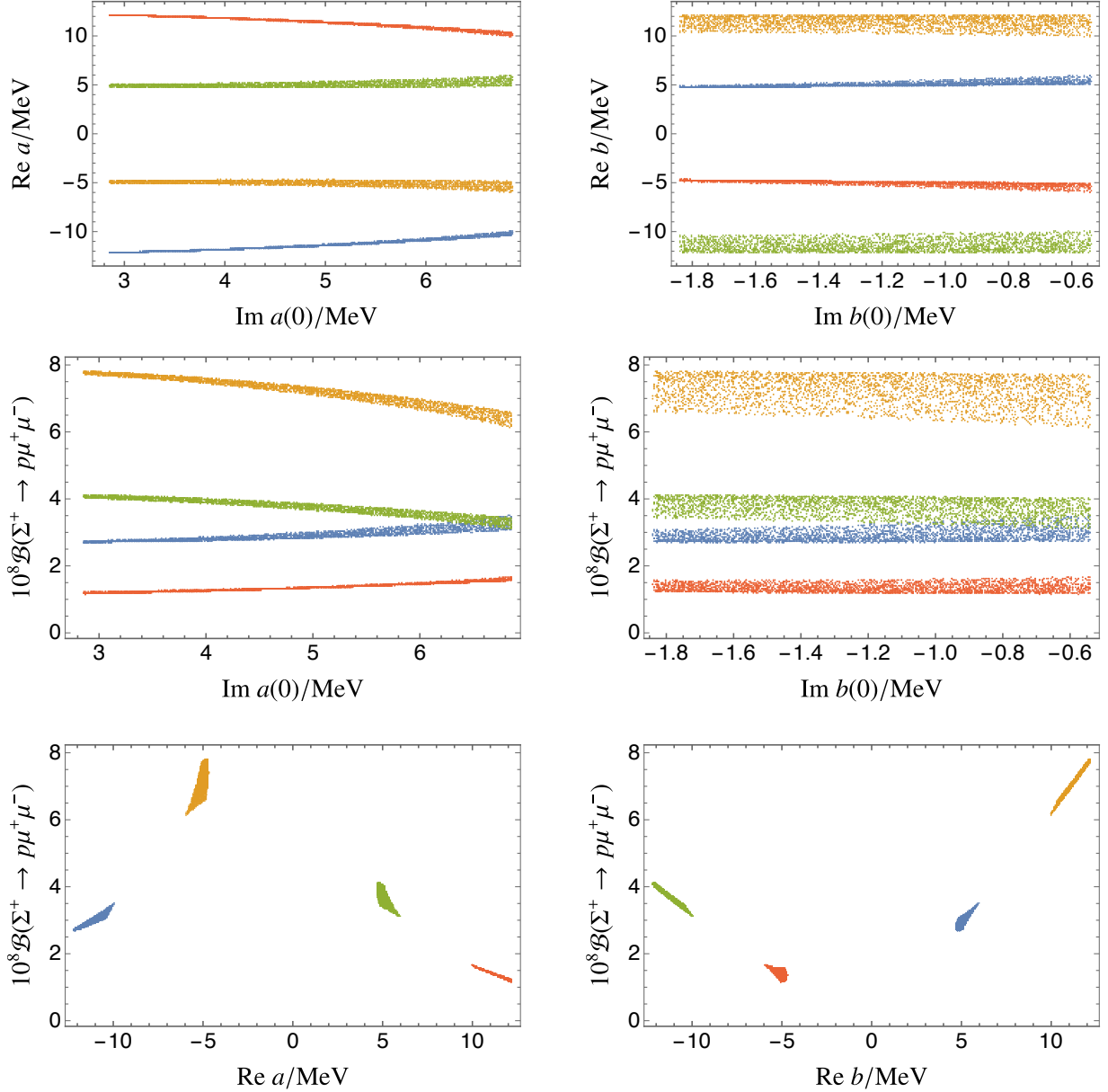


FIG. 1. Variation in the real parts of the form factors  $a$  and  $b$  (top row) and in the resulting branching fraction  $\mathcal{B}(\Sigma^+ \rightarrow p\mu^+\mu^-)$  (middle row) as  $\text{Im } a(0)$  and  $\text{Im } b(0)$  are allowed to vary between the values determined with relativistic baryon  $\chi$ PT and with its heavy-baryon formulation. The bottom plots show the corresponding correlations between  $\mathcal{B}(\Sigma^+ \rightarrow p\mu^+\mu^-)$  and the real parts of  $a$  and  $b$ .

in the third column of the table, is still compatible with the PDG value at the two-sigma level [61] if both of their errors are taken into account. We expect that the situation will become clearer [61] when an improved result from LHCb becomes available in the near future. [61]

Measurements of the branching fraction of  $\Sigma^+ \rightarrow pe^+e^-$  may offer an additional way to [63] resolve the fourfold ambiguity. In this mode, the dominance of the LD contributions is more [63] pronounced, owing to the fact that the  $a$  and  $b$  terms in the amplitude are much enhanced at low [63] values of the dielectron invariant mass,  $M_{ee} = \sqrt{q^2} \geq 2m_e$ . As a consequence, the predictions [63] for  $\mathcal{B}_{ee} = \mathcal{B}(\Sigma^+ \rightarrow pe^+e^-)$  corresponding to the various solutions are similar to one another, as [63] can be seen in the sixth column of Table I. Nevertheless, the difference between solutions can be [63] magnified by raising the minimum of  $M_{ee}$ . This might be achieved by applying, for instance, the [63] cut  $M_{ee} \geq 100$  MeV, leading to the numbers in the last column of Table I. Thus, the selection [63] of an appropriate lower bound on  $M_{ee}$  could make the predictions of the different solutions more [63] distinguishable. This point is further illustrated by Fig. 2. Although the implementation of the [63]  $M_{ee\min}$  cut has a price, which is a decreased rate, the latter may still be within the sensitivity [63] reach of BESIII [2] and LHCb [3–5], depending on the choice of  $M_{ee\min}$ . [63]

It is worth remarking here that the  $\mathcal{B}_{ee}$  range in the sixth column of Table I is roughly 20% less [64] than the corresponding predictions made in Refs. [8, 38]. This is largely because of our adoption [64] of the BESIII finding of  $\mathcal{B}_\gamma$  quoted in Eq. (10), which is also  $\sim 20\%$  lower than the present PDG [64] average [17]. The empirical information on  $\Sigma^+ \rightarrow pe^+e^-$  is still scarce. From the only existing [64] data, reported in Ref. [22], one can infer  $\mathcal{B}(\Sigma^+ \rightarrow pe^+e^-) = (7.7 \pm 4.6) \times 10^{-6}$  [8],<sup>4</sup> which is far [64] from precise and accommodates well all the  $\mathcal{B}_{ee}$  predictions in the sixth column of Table I. Thus, [65]

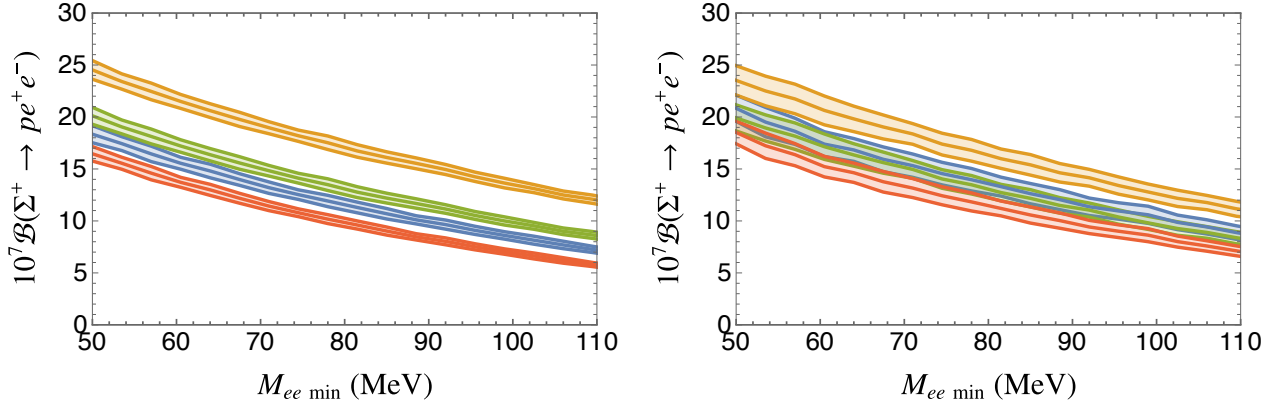


FIG. 2. Dependence of the SM branching fraction of  $\Sigma^+ \rightarrow pe^+e^-$  on a minimum cut in the dielectron [62] invariant mass for the four solutions obtained with relativistic baryon  $\chi$ PT (left plot) and with its [62] heavy-baryon formulation (right plot). In all of the figures in this section, the blue, yellow, green, and [62] red colors correspond to solutions 1, 2, 3, and 4, respectively. The band of each curve in this and the [62] next three figures reflects the ranges of  $\text{Re}(a, b)$  and  $\text{Im}(a(0), b(0))$  for the corresponding solution. [62]

<sup>4</sup> The PDG limit  $\mathcal{B}(\Sigma^+ \rightarrow pe^+e^-) < 7 \times 10^{-6}$  [17] is for neutral currents in this mode and not for its full [64] branching fraction [22].

it goes without saying that the upcoming measurements of  $\Sigma^+ \rightarrow p e^+ e^-$  by BESIII and LHCb<sup>65</sup> can be anticipated to provide highly desirable information pertinent to our study.<sup>65</sup>

Returning to the  $\ell = \mu$  case, one can write the double differential distribution [38, 39]<sup>66</sup>

$$\frac{d^2\Gamma(\Sigma^+ \rightarrow p\mu^+\mu^-)}{dq^2 d(\cos\theta_\mu)} = \left[ \frac{3}{8} \frac{44}{46} (1 + \cos^2\theta_\mu) (1 - f_L) + \mathcal{A}_{FB} \cos\theta_\mu + \frac{3}{4} f_L \sin^2\theta_\mu \right] \frac{d\Gamma(\Sigma^+ \rightarrow p\mu^+\mu^-)}{dq^2} \\ = \mathcal{F}_0 + \mathcal{F}_1 \cos\theta_\mu + \mathcal{F}_2 \cos^2\theta_\mu, \quad (16)$$

where  $\theta_\mu$  stands for the angle between the directions of the  $\mu^-$  and  $p$  in the rest frame of the  $\mu^+\mu^-$  system,  $f_L$  is the fraction of longitudinally polarized dimuons,  $\mathcal{A}_{FB}$  designates the muon forward-backward asymmetry, and  $f_L$ ,  $\mathcal{A}_{FB}$ , and  $\mathcal{F}_{0,1,2}$  are all independent of  $\theta_\mu$ . The expressions for  $\mathcal{F}_{0,1,2}$  in the general parameterization of Eq. (14) can be found in the appendix of Ref. [38].<sup>68</sup>

Thus, explicitly we have [38]<sup>69</sup>

$$\mathcal{A}_{FB} = \frac{\beta^2 \bar{\lambda}}{64\pi^3 \Gamma' m_\Sigma^3} \text{Re} \left\{ \left[ M_+ \tilde{A}^* \tilde{F} - M_- \tilde{B}^* \tilde{E} - (\tilde{A}^* \tilde{G} + \tilde{B}^* \tilde{H}) m_\mu + \tilde{C}^* \tilde{F} + D^* \tilde{E} \right] q^2 \right. \\ \left. - (M_+ \tilde{C}^* \tilde{G} - M_- \tilde{D}^* \tilde{H}) m_\mu \right\}, \quad (17)$$

where<sup>55</sup>

$$\Gamma' \equiv \frac{d\Gamma(\Sigma^+ \rightarrow p\mu^+\mu^-)}{dq^2} = 2\mathcal{F}_0 + \frac{2}{3}\mathcal{F}_2, \quad \beta = \sqrt{1 - \frac{4m_\mu^2}{q^2}}, \quad (18)$$

$$\bar{\lambda} = (M_+^2 - q^2)(M_-^2 - q^2), \quad M_\pm = m_\Sigma \pm m_p.$$

Since  $\tilde{A}$ ,  $\tilde{B}$ ,  $\tilde{C}$ , and  $\tilde{D}$  are dominated by the LD contributions, while  $\tilde{E}$ ,  $\tilde{F}$ ,  $\tilde{G}$ , and  $\tilde{H}$  are not,<sup>73</sup>  $\mathcal{A}_{FB}$  is potentially sensitive to NP which can enhance one or more of the latter set of quantities<sup>73</sup> significantly compared to their SM expectations. Also of interest is the integrated forward-backward asymmetry<sup>259</sup>

$$\tilde{A}_{FB} = \frac{1}{\Gamma(\Sigma^+ \rightarrow p\mu^+\mu^-)} \int \Gamma' \mathcal{A}_{FB} dq^2, \quad (19)$$

where both the numerator and denominator of  $\tilde{A}_{FB}$  are to be evaluated for the same solution.<sup>75</sup> The SM prediction for  $\tilde{A}_{FB}$  can be viewed in the fifth column of Table I, and its differential distribution,<sup>75</sup>

$$\frac{d\tilde{A}_{FB}}{dM_{\mu\mu}} = \frac{2\Gamma' \mathcal{A}_{FB} M_{\mu\mu}}{\Gamma(\Sigma^+ \rightarrow p\mu^+\mu^-)}, \quad (20)$$

versus the dimuon invariant mass  $M_{\mu\mu} = \sqrt{q^2}$  is depicted in Fig. 3. Evidently, there is a sign flip for two of the solutions (distributions 1 and 2 in both the relativistic and heavy-baryon cases<sup>77</sup> become negative).<sup>77</sup>

Another important quantity is the dimuon spectrum given by<sup>80</sup>

$$\frac{1}{\hat{\Gamma}} \frac{d\hat{\Gamma}}{dM_{\mu\mu}} = \frac{2\Gamma' M_{\mu\mu}}{\hat{\Gamma}}, \quad \hat{\Gamma} \equiv \Gamma(\Sigma^+ \rightarrow p\mu^+\mu^-), \quad (21)$$

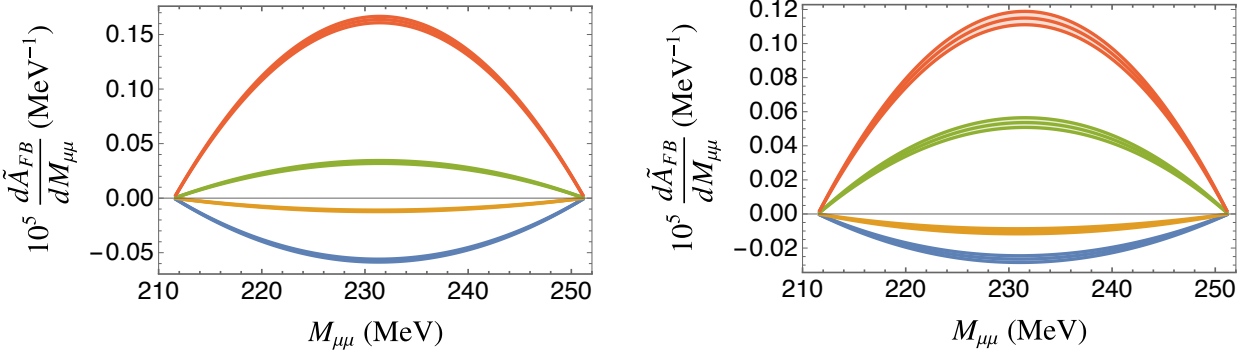


FIG. 3. The differential  $\tilde{A}_{FB}$  distribution in  $\Sigma^+ \rightarrow p\mu^+\mu^-$  versus the dimuon invariant mass,  $M_{\mu\mu}$ , for [79] the four relativistic (left) and heavy-baryon (right) solutions in the SM. [79]

hence also normalized by the rate. The dependence of  $(d\hat{\Gamma}/dM_{\mu\mu})/\hat{\Gamma}$  on  $M_{\mu\mu}$  for each of the [82] solutions is illustrated in Fig. 4. It can be seen that the spectrum for solution 4, in both the [82] relativistic and heavy-baryon cases, peaks at lower  $M_{\mu\mu}$  than the other three. [82]

From the two lines in Eq. (16), it is straightforward to realize that the fraction  $f_L$  of longitudinally [83] polarized dimuons is related to  $\mathcal{F}_{0,2}$  by [83]

$$f_L = \frac{2}{3\hat{\Gamma}} (\mathcal{F}_0 - \mathcal{F}_2), \quad (22)$$

where  $\hat{\Gamma}' = 2\mathcal{F}_0 + 2\mathcal{F}_2/3$  with the  $\mathcal{F}_0$  term being numerically dominant, as detailed in Ref. [38]. [85]  
We can then define the integrated form [85]

$$\hat{f}_L = \frac{1}{\hat{\Gamma}} \int \hat{\Gamma}' f_L q^2 = \frac{4}{3\hat{\Gamma}} \int (\mathcal{F}_0 - \mathcal{F}_2) M_{\mu\mu} dM_{\mu\mu}. \quad (23)$$

In Fig. 5 we display  $d\hat{f}_L/dM_{\mu\mu}$  versus  $M_{\mu\mu}$ . This distribution mostly mimics the dimuon spectrum [87] in Fig. 4, which is expected due to the numerical smallness of  $\mathcal{F}_2$  relative to  $\mathcal{F}_0$  within the SM. [87]  
It is interesting to mention that experimentally it may be possible to extract  $f_L$  from Eq. (16), [87]  
as was done for  $\Lambda_b \rightarrow \Lambda\mu^+\mu^-$  by LHCb [39]. [87]

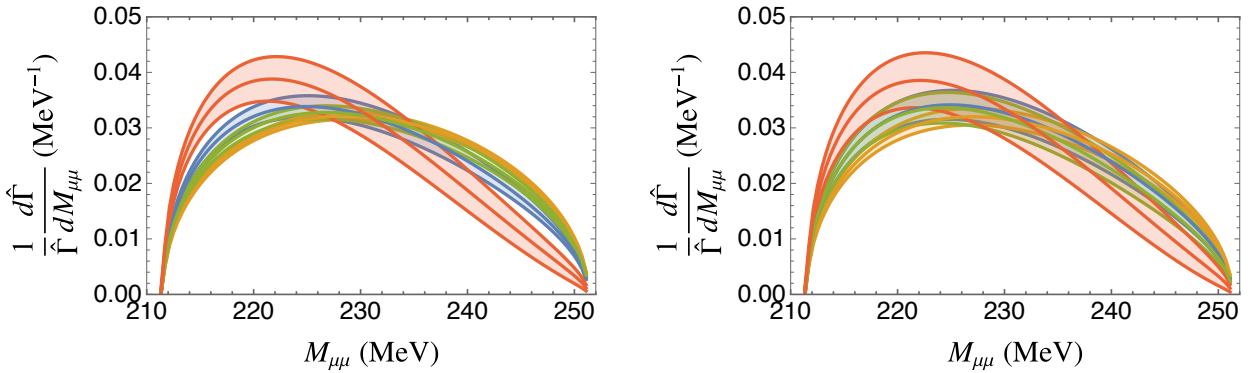


FIG. 4. The dimuon spectrum in  $\Sigma^+ \rightarrow p\mu^+\mu^-$  versus the dimuon invariant mass for the four relativistic [78] (left) and heavy-baryon (right) solutions in the SM. [78]

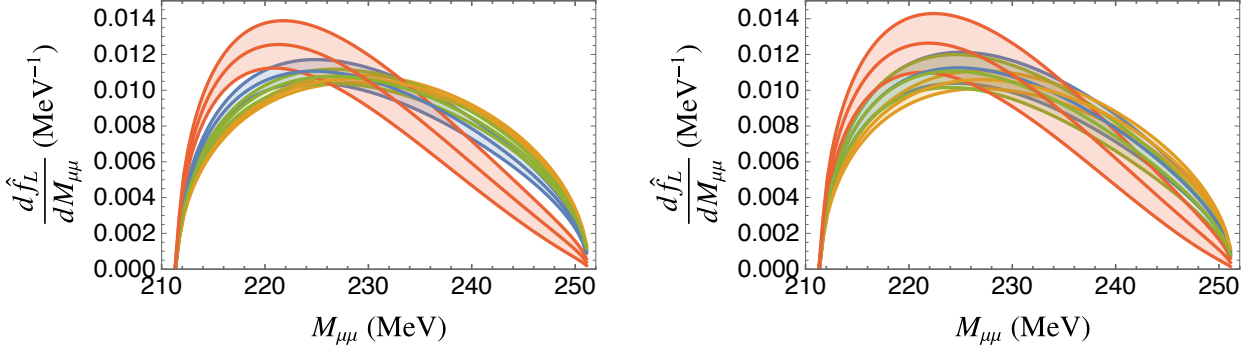


FIG. 5. The  $\hat{f}_L$  distributions in  $\Sigma^+ \rightarrow p\mu^+\mu^-$  in the SM normalized to their corresponding rate for the four relativistic (left) and heavy-baryon (right) solutions.<sup>88</sup>

## V. NEW PHYSICS CONTRIBUTIONS<sup>89</sup>

To take into account the effects of new physics beyond the SM, we work with the effective Hamiltonian<sup>90</sup>

$$\mathcal{H}_{\text{eff}} = - \sum_i \mathcal{C}_i \mathcal{O}_i + \text{H.c.}, \quad (24)$$

<sup>91</sup>  
<sup>202</sup>

where the operators  $\mathcal{O}_i$  are defined as<sup>92</sup>

$\mathcal{O}_7 = \frac{\lambda_t G_F}{\sqrt{2}} \frac{e m_s}{4\pi^2} \bar{s}_R \sigma^{\kappa\nu} d_L F_{\kappa\nu},$ $\mathcal{O}_9^\ell = \frac{\lambda_t G_F}{\sqrt{2}} \frac{e^2}{4\pi^2} \bar{s}_L \gamma^\nu d_L \bar{\ell} \gamma_\nu \ell,$ $\mathcal{O}_{10}^\ell = \frac{\lambda_t G_F}{\sqrt{2}} \frac{e^2}{4\pi^2} \bar{s}_L \gamma^\nu d_L \bar{\ell} \gamma_\nu \gamma_5 \ell,$ $\mathcal{O}_S = \frac{\lambda_t G_F}{\sqrt{2}} \frac{e^2 m_s}{4\pi^2} \bar{s}_L d_R \bar{\ell} \ell,$ $\mathcal{O}_P = \frac{\lambda_t G_F}{\sqrt{2}} \frac{e^2 m_s}{4\pi^2} \bar{s}_L d_R \bar{\ell} \gamma_5 \ell,$	$\mathcal{O}_{7'} = \frac{\lambda_t G_F}{\sqrt{2}} \frac{e m_s}{4\pi^2} \bar{s}_L \sigma^{\kappa\nu} d_R F_{\kappa\nu},$ $\mathcal{O}_{9'}^\ell = \frac{\lambda_t G_F}{\sqrt{2}} \frac{e^2}{4\pi^2} \bar{s}_R \gamma^\nu d_R \bar{\ell} \gamma_\nu \ell,$ $\mathcal{O}_{10'}^\ell = \frac{\lambda_t G_F}{\sqrt{2}} \frac{e^2}{4\pi^2} \bar{s}_R \gamma^\nu d_R \bar{\ell} \gamma_\nu \gamma_5 \ell,$ $\mathcal{O}_{S'} = \frac{\lambda_t G_F}{\sqrt{2}} \frac{e^2 m_s}{4\pi^2} \bar{s}_R d_L \bar{\ell} \ell,$ $\mathcal{O}_{P'} = \frac{\lambda_t G_F}{\sqrt{2}} \frac{e^2 m_s}{4\pi^2} \bar{s}_R d_L \bar{\ell} \gamma_5 \ell,$
--	---

<sup>93</sup>

(25)

with  $f_{L,R} = P_{L,R} f$  for fermion  $f$  and  $\lambda_q = V_{qd} V_{qs}^*$ . For the Wilson coefficients  $\mathcal{C}_i$  in Eq. (24), we explicitly separate any SM contribution to them by writing  $\mathcal{C}_i = C_i^{\text{SM}} + C_i$ , where " $C_i$ " designates the part induced by NP. Since we consider only NP that preserves  $CP$  symmetry, we suppose that the products  $\lambda_j C_i$ , which occur in  $\mathcal{H}_{\text{eff}}$ , are real numbers. As seen below, the  $C_i$  enter the kaon observables of interest as either of  $C_{j\pm} \equiv (C_j \pm C_{j'})$ ,  $j = 7, 9, 10, S, P$ , and so we will adopt those combinations.<sup>94</sup>

From the H.c. part of  $\mathcal{H}_{\text{eff}}$  in Eq. (24), the NP contributions to  $\Sigma^+ \rightarrow p\ell^+\ell^-$  are [95]

$$\begin{aligned}\tilde{A} &= \frac{\lambda_t G_F}{\sqrt{2}} \frac{e^2 m_s}{4\pi^2 q^2} c_\sigma C_{7+}, & \tilde{B} &= \frac{\lambda_t G_F}{\sqrt{2}} \frac{e^2 m_s}{4\pi^2 q^2} c_\sigma C_{7-}, \\ \tilde{C} &= \frac{-\lambda_t G_F}{\sqrt{2}} \frac{e^2}{8\pi^2} C_{9+}, & \tilde{D} &= \frac{\lambda_t G_F}{\sqrt{2}} \frac{e^2}{8\pi^2} (F - D) C_{9-}, \\ \tilde{E} &= \frac{\lambda_t G_F}{\sqrt{2}} \frac{e^2}{8\pi^2} C_{10+}, & \tilde{F} &= \frac{\lambda_t G_F}{\sqrt{2}} \frac{e^2}{8\pi^2} (D - F) C_{10-}, \\ \tilde{G} &= \frac{\lambda_t G_F}{\sqrt{2}} \frac{e^2 m_s}{8\pi^2} \left( \frac{m_\Sigma - m_p}{m_s - m_d} \right) C_{S+}, & \tilde{J} &= \frac{\lambda_t G_F}{\sqrt{2}} \frac{e^2 m_s}{8\pi^2} \left( \frac{m_\Sigma - m_p}{m_d - m_s} \right) C_{P+},\end{aligned}\quad (26)$$

165

and [1]

$$\begin{aligned}\tilde{H} &= \frac{\lambda_t G_F}{\sqrt{2}} \frac{e^2 m_s}{8\pi^2} \left( \frac{m_\Sigma + m_p}{m_{K^0}^2 - q^2} \right) \frac{m_{K^0}^2}{m_d + m_s} (D - F) C_{S-}, \\ \tilde{K} &= \frac{\lambda_t G_F}{\sqrt{2}} \frac{e^2}{8\pi^2} \left( \frac{m_\Sigma + m_p}{q^2 - m_{K^0}^2} \right) (D - F) \left( 2C_{10-} m_\ell + \frac{C_{P-} m_{K^0}^2 m_s}{m_d + m_s} \right),\end{aligned}\quad (27)$$

45  
98

where the relation  $\lambda_t^* C_i^* = \lambda_t C_i$  has been applied, which is valid for  $\text{Im}(\lambda_t C_i) = 0$ . In numerical work we set  $e^2 = 4\pi\alpha_e(0)$  for the  $a, b, c$ , and  $d$  terms in Eq. (15), which arise from photon-exchange LD effects, and  $e^2 = 4\pi\alpha_e(m_Z)$  in the rest of Eq. (15) and in Eqs. (26)-(27). [99]

The complete numerical expression for  $\mathcal{B}(\Sigma^+ \rightarrow p\mu^+\mu^-)$  can be written as [100]

$$\mathcal{B}(\Sigma^+ \rightarrow p\mu^+\mu^-)_i = \left[ \text{SM}_i + \sum_{j,k} n_{ij} (\lambda_t C_j) + 10^{-2} \sum_{jk} q_{jk} (\lambda_t C_j)(\lambda_t C_k) \right] \times 10^{-8}, \quad (28)$$

101

where  $\text{SM}_i$  refers to each of the four solutions derived with relativistic baryon  $\chi$ PT and with its heavy-baryon formulation. The terms linear in the Wilson coefficients (WCs) representing NP arise from interference with the SM and are therefore different for each case. These terms are largest when the WCs interfere with the SM long-distance component. The part quadratic in the WCs,  $C_j C_k$ , originate purely from NP and are thus the same for all four solutions. We display our numerical results for  $n_{ij}$  and  $q_{jk}$  in Tables II and III,<sup>5</sup> respectively. These numbers indicate that, with  $\lambda_t$  multiplying each WC in Eq. (28), the dimensionless ones, such as  $C_{7-}$  and  $C_{9-}$ , must be at least a few times  $10^2$  in size to modify the SM rates at the percent level or higher.<sup>6</sup> [102]

We now turn our attention to the integrated forward-backward asymmetry as defined in Eq. (19) in the presence of NP. The decay rate that normalizes this asymmetry also varies when there is NP, as per Eq. (28), but we present results that include the NP terms only in the

<sup>5</sup> Ref. [40] gives a result that includes only the  $C_{9+}^2$  and  $C_{9-}^2$ . Our numbers disagree with theirs by factors of two. Converting their result to our notation, they find coefficients 1.94 for  $C_{9+}^2$  and 0.94 for  $C_{9-}^2$  instead of our 0.972 and 2.06, respectively, from Table III. [102]

<sup>6</sup> Equivalently, only NP arising from ultraviolet models without a mixing angle suppression similar to  $\lambda_t$  can measurably affect this rate. [102]

Solution	SM <sub>i</sub>	C <sub>7+</sub>	C <sub>7-</sub>	C <sub>9+</sub>	C <sub>9-</sub>	103
Rel 1	2.7	-0.070	0.34	0.046	0.37	103
Rel 2	7.8	-0.028	0.71	0.026	0.77	103
Rel 3	4.2	0.025	-0.50	-0.0008	-0.55	
Rel 4	1.2	0.067	-0.14	-0.021	-0.15	
HB 1	3.6	-0.057	0.40	0.040	0.44	
HB 2	6.2	-0.035	0.59	0.029	0.65	
HB 3	3.2	0.032	-0.39	-0.0043	-0.42	
HB 4	1.8	0.054	-0.20	-0.015	-0.21	103

TABLE II. Numerical coefficients SM<sub>i</sub> and n<sub>ij</sub> appearing in Eq. (28). 104

C <sub>7+</sub> <sup>2</sup>	C <sub>7-</sub> <sup>2</sup>	C <sub>9+</sub> <sup>2</sup>	C <sub>9-</sub> <sup>2</sup>	C <sub>10+</sub> <sup>2</sup>	C <sub>10-</sub> <sup>2</sup>	C <sub>S+</sub> <sup>2</sup>	C <sub>S-</sub> <sup>2</sup>	C <sub>P+</sub> <sup>2</sup>	C <sub>P-</sub> <sup>2</sup>	105
0.194	1.73	0.972	2.06	5.6	0.41	0.06 GeV <sup>2</sup>	0.0013 GeV <sup>2</sup>	0.353 GeV <sup>2</sup>	0.01 GeV <sup>2</sup>	

C <sub>7+</sub> C <sub>9+</sub>	C <sub>7-</sub> C <sub>9-</sub>	C <sub>10+</sub> C <sub>P+</sub>	C <sub>10-</sub> C <sub>P-</sub>	106
-0.193	3.75	-2.78 GeV	0.082 GeV	106

TABLE III. Numerical coefficients q<sub>jk</sub> appearing in Eq. (28).

numerator of the asymmetry. The rationale for this choice is that this observable will only be 108 measured after the decay rate is known. With this in mind, we write for the terms that arise 108 from interference with the LD SM contribution as 108

$$\begin{aligned} \tilde{A}_{\text{FB}} &= \frac{1}{\Gamma(\Sigma^+ \rightarrow p\mu^+\mu^-)} \int \Gamma' \mathcal{A}_{\text{FB}} dq^2 \\ &\supset [a_{10+} (\lambda_t C_{10+}) + a_{10-} (\lambda_t C_{10-}) + a_{S+} \text{GeV} (\lambda_t C_{S+}) + a_{S-} \text{GeV} (\lambda_t C_{S-})] \times 10^{-2}, \end{aligned} \quad (29) \quad 109$$

where the coefficients a<sub>i</sub> for the four relativistic solutions and their heavy-baryon counterparts 110 are tabulated in Table IV.<sup>7</sup> With NP coefficients of order 10<sup>2</sup>, their impact is to cause  $\tilde{A}_{\text{FB}}$  to 110 exceed its SM expectations by a factor of ten already. 110

Solution	a <sub>10+</sub>	a <sub>10-</sub>	a <sub>S+</sub>	a <sub>S-</sub>	111
Rel 1	-0.22 ± 0.01	-1.18 ± 0.02	0.082 ± 0.001	-0.092 ± 0.006	
Rel 2	-0.158 ± 0.003	-0.16 ± 0.01	0.020 ± 0.001	-0.065 ± 0.001	
Rel 3	0.214 ± 0.005	0.29 ± 0.03	0.015 ± 0.001	0.083 ± 0.002	
Rel 4	0.20 ± 0.03	2.54 ± 0.05	-0.003 ± 0.002	0.07 ± 0.01	
HB 1	-0.19 ± 0.02	-0.70 ± 0.04	0.054 ± 0.001	-0.081 ± 0.007	
HB 2	-0.16 ± 0.01	-0.26 ± 0.03	0.026 ± 0.001	-0.067 ± 0.003	
HB 3	0.21 ± 0.01	0.47 ± 0.06	0.016 ± 0.002	0.078 ± 0.006	
HB 4	0.20 ± 0.03	1.36 ± 0.08	0.010 ± 0.003	0.07 ± 0.01	111

TABLE IV. Coefficients a<sub>i</sub> in Eq. (19) for the integrated forward-backward asymmetry. 112

<sup>7</sup> These numbers appear in Ref. [40] for one relativistic solution, and when converted to our conventions they 110 disagree with ours. That reference comments that this is due to the use of different form factors. 110

The additional terms in  $\tilde{A}_{\text{FB}}$ , besides those in the second line of Eq. (29), are expressible as 113

$$\Gamma(\Sigma^+ \rightarrow p\mu^+\mu^-) \tilde{A}_{\text{FB}} \supset \sum_{ij} \tilde{q}_{ij} (\lambda_t C_i)(\lambda_t C_j) \times 10^{-25}, \quad (30)$$

114

and therefore the parameters  $\tilde{q}_{ij}$  are independent of the SM LD effects. Our numerical results 115  
for  $\tilde{q}_{ij}$  can be viewed in Table V. 115

$C_{7+}C_{10-}$	$C_{7+}C_{S+}$	$C_{7-}C_{10+}$	$C_{7-}C_{S-}$	$C_{9+}C_{10-}$	$C_{9+}C_{S+}$	$C_{9-}C_{10+}$	$C_{9-}C_{S-}$
1.5	-0.052 GeV	-0.49	-0.20 GeV	-0.51	1.5 GeV	-0.51	-0.24 GeV

TABLE V. Numerical coefficients  $\tilde{q}_{ij}$  appearing in Eq. (30).

## VI. KAON OBSERVABLES 178

### A. SM Wilson coefficients 119

The kaon modes affected by the quark-level transition  $s \rightarrow d\mu^+\mu^-$  are also dominated by long-distance contributions within the SM. This makes it very difficult to extract precise information 120  
on the SM short-distance parameters, or, indeed, new physics. Nevertheless, the corresponding 120  
kaon data can serve as useful constraints on NP which is large enough to measurably affect the 120  
 $\Sigma^+ \rightarrow p\mu^+\mu^-$  rate. The SM SD contributions enter these modes via the Wilson coefficients, at 120  
the scale  $\mu = 1 \text{ GeV}$ . 121

$$C_7^{\text{SM}} = \frac{-\lambda_u}{2\lambda_t} C_{7\gamma}, \quad C_9^{\text{SM}} = \frac{2\pi}{\alpha_e} \left( y_{7V} - \frac{\lambda_u}{\lambda_t} z_{7V} \right), \quad C_{10}^{\text{SM}} = \frac{2\pi}{\alpha_e} y_{7A}. \quad (31)$$

Numerically we employ  $z_{7V} = -0.046\alpha_e$ ,  $y_{7V} = 0.73\alpha_e$ , and  $y_{7A} = -0.68\alpha_e$ , as before.<sup>8</sup> 122

### B. Relevant kaon modes 123

We begin with the modes  $K_{L,S} \rightarrow \mu^+\mu^-$ . For our numerical study, we employ the expressions 124  
for all contributions to these two rates that exist in the public SuperIso code [42, 43]. In both 124  
cases, the LD contribution is dominated by a two-photon intermediate state. Its extraction relies 124  
on the measured  $K_{L,S} \rightarrow \gamma\gamma$  rates supplemented with hadronic models. The LD contributions 124  
to  $K_{L,S} \rightarrow \mu^+\mu^-$  are therefore potentially contaminated by NP entering through  $C_{7,7'}$ . This has 124  
been considered in the literature, and we will later list the corresponding constraints obtained 124  
in Ref. [44], on Table VII. There are several proposals to improve these measurements [7]. 124

<sup>8</sup> The error in these coefficients is sometimes quantified as  $y_{7V} = (0.73 \pm 0.04)\alpha_e$  and  $y_{7A} = (-0.68 \pm 0.03)\alpha_e$  122  
with the uncertainty range arising from taking  $\bar{m}_t(m_t) = (167 \pm 5) \text{ GeV}$  and  $0.8 \leq \mu/\text{GeV} \leq 1.2$  [41]. 64

### 1. $K_L \rightarrow \mu^+ \mu^-$

This mode receives a SD contribution proportional to  $\text{Re } C_{10}^{\text{SM}}$ , but the rate is dominated by the aforesaid LD contribution from a two-photon intermediate state. The absorptive part of this LD contribution is determined by the measured rate of  $K_L \rightarrow \gamma\gamma$ , and the difference between this rate and the absorptive contribution can be attributed to a combination of a model-dependent LD dispersive contribution, a SM SD contribution, and NP. The branching fraction in relation to all of them can be parameterized as [18, 45]

$$\begin{aligned}\mathcal{B}(K_L^0 \rightarrow \mu^+ \mu^-) &= \tau_{K_L} \frac{f_K^2 m_{K^0}^3 \beta_{\mu, K}}{16\pi} (|N_L^{\text{LD}} + A_L^{\text{SM}} + A_L^{\text{NP}}|^2 + \beta_{\mu, K}^2 |B_L|^2), \\ N_L^{\text{LD}} &= \pm [0.54(77) - 3.95i] \times 10^{-11} \text{ GeV}^{-2}, \\ A_L^{\text{SM}} &= \frac{G_F \alpha_e}{\sqrt{2}\pi} \frac{2m_\mu}{m_{K^0}} \left( \frac{Y_c}{s_W^2} \text{Re } \lambda_c + \frac{Y(x_t)}{s_W^2} \text{Re } \lambda_t \right) \text{[45]} \\ A_L^{\text{NP}} &= \frac{-G_F \alpha_e}{\sqrt{2}\pi} \text{Re} \left[ \frac{2m_\mu}{m_{K^0}} (\lambda_t C_{10-}) + \frac{m_{K^0} m_s}{m_s + m_d} (\lambda_t C_{P-}) \right], \\ B_L &= \frac{G_F \alpha_e}{\sqrt{2}\pi} \frac{m_{K^0} m_s}{(m_s + m_d)} \text{Im} (\lambda_t C_{S-}).\end{aligned}\quad (32) \quad 108$$

Recall that we are assuming no  $CP$  violation in the NP for our numerical study, implying that we set  $B_L = 0$ . We have explicitly separated the SM SD contribution,  $A_L^{\text{SM}}$  [46], so that  $C_{10}$  refers to NP only.

### 2. $K_S \rightarrow \mu^+ \mu^-$

This mode also has SD and LD components entering the branching fraction as [18, 45]

$$\begin{aligned}\mathcal{B}(K_S^0 \rightarrow \mu^+ \mu^-) &= \tau_{K_S} \frac{f_K^2 m_{K^0}^3 \beta_{\mu, K}}{16\pi} (\beta_{\mu, K}^2 |N_S^{\text{LD}} - A_S^{\text{NP}}|^2 + |B_S^{\text{SM}} + B_S^{\text{NP}}|^2), \\ N_S^{\text{LD}} &= (-2.65 + 1.14i) \times 10^{-11} \text{ GeV}^{-2}, \\ A_S^{\text{NP}} &= \frac{G_F \alpha_e}{\sqrt{2}\pi} \frac{m_{K^0} m_s}{(m_s + m_d)} \text{Re} (\lambda_t C_{S-}), \\ B_S^{\text{SM}} &= \frac{G_F \alpha_e}{\sqrt{2}\pi} \frac{2m_\mu}{m_{K^0}} \text{Im} \left( \frac{-Y_c}{s_W^2} \lambda_c - \frac{Y(x_t)}{s_W^2} \lambda_t \right) \text{[45]} \\ B_S^{\text{NP}} &= \frac{G_F \alpha_e}{\sqrt{2}\pi} \left[ \frac{2m_\mu}{m_{K^0}} \text{Im} (\lambda_t C_{10-}) + \frac{m_{K^0} m_s}{m_s + m_d} \text{Im} (\lambda_t C_{P-}) \right].\end{aligned}\quad (33) \quad 131$$

Again, we have explicitly written the SM SD contribution through  $C_{10}$  as  $B_S^{\text{SM}}$ . In the scenario with no  $CP$  violation in the NP,  $B_S^{\text{NP}} = 0$ .

### 3. $K_{L,S} \rightarrow \pi^0 \ell^+ \ell^-$

Within the SM these modes are predominantly  $CP$ -violating and receive multiple contributions. There are direct and through-mixing  $CP$ -violating contributions as well as interference

between them,  $C_{\text{dir}}^{\ell\ell}$ ,  $C_{\text{mix}}^{\ell\ell}$  and  $C_{\text{int}}^{\ell\ell}$  respectively. Theoretical considerations suggest that the sign of the interference term is plus [47]. There is also a LD  $CP$ -conserving contribution dominated by a two-photon intermediate state,<sup>9</sup>  $C_{\gamma\gamma}^{\ell\ell}$ . Potentially there are NP contributions as well, which we include following Ref. [48]. Some enter  $C_{\text{dir}}^{\ell\ell}$  and others we dub  $C_{\text{NP}}^{\ell\ell}$ . A practical complication when using these modes to constrain NP is that two contributions are extracted from experiment. The  $CP$ -conserving contribution is partially extracted from  $K_L \rightarrow \pi^0 \gamma\gamma$  and as such is potentially contaminated by NP through  $C_{7,7'}$ . We partially address this issue by using the constraints on  $C_7$  and  $C_{7'}$  as obtained from the  $K \rightarrow \pi\pi\gamma$  and  $K \rightarrow \gamma\gamma$  modes [44], respectively. The  $CP$ -violating contribution through mixing relies on the measurement of  $K_S \rightarrow \pi^0 \ell^+ \ell^-$ , and NP affecting those modes could contaminate the extracted value of  $a_S$ . However, an  $a_S$  representing LD contributions is the same for both the electron and muon modes, so that the difference between the two extractions can be attributed to NP that breaks lepton flavor universality (LFU).

We follow Refs. [41, 47–49] to write<sup>10</sup>

$$\mathcal{B}(K_L \rightarrow \pi^0 \ell\bar{\ell}) = (C_{\text{NP}}^{\ell\ell} + C_{\text{dir}}^{\ell\ell} \pm C_{\text{int}}^{\ell\ell} |a_S| + C_{\text{mix}}^{\ell\ell} |a_S|^2 + C_{\gamma\gamma}^{\ell\ell}) \times 10^{-12}. \quad (34)$$

As the expressions below imply, NP contributions may enter the rate through the term  $C_{\text{NP}}^{\ell\ell}$  via the coefficients  $C_{P+}$  and  $C_{S+}$  and also through the term  $C_{\text{dir}}^{\ell\ell}$  via the coefficients  $C_{9+}$  and  $C_{10+}$ .

To exhibit the dependence of the first three terms in Eq. (34) on the possible NP, we follow Refs. [48, 49] and write<sup>10</sup>

$$\begin{aligned} C_{\text{NP}}^{\mu\mu} &= 10^8 \text{Im}(\lambda_t C_{P+} \text{GeV}) \{0.09 \text{Im} \lambda_t + [0.0039 \text{Im}(\lambda_t C_{P+} \text{GeV}) - 0.02 \text{Im}(\lambda_t C_{10+})]\}, \\ &\quad + 10^4 \text{Re}(\lambda_t C_{S+} \text{GeV}) [-0.027(7) + 0.0019 \times 10^4 \text{Re}(\lambda_t C_{S+} \text{GeV})], \\ C_{\text{dir}}^{\mu\mu} &= 10^8 \{0.033 [\text{Im}(\lambda_t C_{10+}) - 4.27(19) \text{Im} \lambda_t]^2 + 0.014 [\text{Im}(\lambda_t C_{9+}) + 4.59(25) \text{Im} \lambda_t]^2\}, \\ C_{\text{int}}^{\mu\mu} &= 10^4 [1.37(8) \text{Im} \lambda_t + 0.3 \text{Im}(\lambda_t C_{9+})], \\ C_{\text{NP}}^{ee} &= 10^8 \text{Im}(\lambda_t C_{P+} \text{GeV}) \{0.0013 \text{Im} \lambda_t + [0.0076 \text{Im}(\lambda_t C_{P+} \text{GeV}) - 0.0003 \text{Im}(\lambda_t C_{10+})]\}, \\ &\quad + 10^4 \text{Re}(\lambda_t C_{S+} \text{GeV}) [-0.021(4) + 0.0077 \times 10^4 \text{Re}(\lambda_t C_{S+} \text{GeV})], \\ C_{\text{dir}}^{ee} &= 0.06 \times 10^8 \{[\text{Im}(\lambda_t C_{10+}) - 4.27(19) \text{Im} \lambda_t]^2 + [\text{Im}(\lambda_t C_{9+}) + 4.59(25) \text{Im} \lambda_t]^2\}, \\ C_{\text{int}}^{ee} &= 10^4 [5.84(35) \text{Im} \lambda_t + 1.28 \text{Im}(\lambda_t C_{9+})], \end{aligned} \quad (35)$$

where the terms linear in  $\text{Re} C_{S+}$  arise from interference with the two-photon contribution. In Eq. (35) the explicit factors of  $10^4$  and  $10^8$  appear from the practice of writing this result in terms of  $10^4 \lambda_t$ . In addition, the last two terms in Eq. (34) are given by

$$C_{\text{mix}}^{\mu\mu} = 3.36 \pm 0.20, \quad C_{\gamma\gamma}^{\ell\ell} = 5.2 \pm 1.6, \quad C_{\text{mix}}^{ee} = 14.5 \pm 0.5, \quad C_{\gamma\gamma}^{ee} \approx 0. \quad (36)$$

<sup>9</sup> For our numerical studies we will use the expressions for these modes as coded for **SuperIso** and provided to us by F. Mahmoudi.

<sup>10</sup> It is to be understood that the WCs contributing to the various dielectron and dimuon observables need to have superscripts  $\ell\ell = ee$  and  $\mu\mu$ , respectively, if LFU is absent and the two types of WCs occur together and are both nonzero, as in a few instances discussed below. In our numerical analysis in Sec. VII we assume that only the  $\ell = \mu$  WCs contain NP.

In the scenario we are pursuing here, where the NP is  $CP$  conserving, these results indicate that [142](#)  
 $C_{S+}$  is the only WC that can be constrained by these modes. [142](#)

However, it is also possible for NP to contaminate the extraction of the parameter  $a_S$ , and [143](#)  
in that way a constrain on  $C_{9+}$  arises. The parameter  $a_S$  can be inferred from measurements [143](#)  
of  $K_S \rightarrow \pi^0 \ell^+ \ell^-$ . Those modes, in turn, are LD dominated and parameterized in  $\chi$ PT with [143](#)  
the constants  $a_S$  and  $b_S$  which are then extracted from experiment [\[50, 51\]](#). Early extractions [143](#)  
assuming LFU suggested the value  $|a_S| = 1.20 \pm 0.20$  [\[41\]](#), whereas more recent studies suggest [143](#)  
a larger error,  $|a_S| = 1.3 \pm 3.2$  [\[52\]](#). [143](#)

A contamination from NP can only be extracted from these if it violates LFU. The separate [144](#)  
measurements of  $a_S$  in the muon and electron modes start from the  $\chi$ PT parameterization of the [144](#)  
LD SM branching fractions given by [\[53\]](#) [144](#)

$$\begin{aligned} \mathcal{B}(K_S \rightarrow \pi^0 e^+ e^-) &= (0.01 - 0.55a_S - 0.17b_S + 43.76a_S^2 + 11.83a_S b_S + 1.28b_S^2) \times 10^{-10}, \\ \mathcal{B}(K_S \rightarrow \pi^0 \mu^+ \mu^-) &= (0.07 - 3.96a_S - 1.34b_S + 86.90a_S^2 + 50.21a_S b_S + 7.66b_S^2) \times 10^{-11}. \end{aligned} \quad (37) \quad 145$$

Existing measurements do not have enough information to determine both  $a_S$  and  $b_S$ , and so [146](#)  
predictions rely on a vector-meson-dominance model leading to  $b_S/a_S = m_K^2/m_\rho^2$  [\[51\]](#). Using [146](#)  
this form, the experimental collaborations have extracted a value for  $a_S$  from each of the two [146](#)  
modes [\[54, 55\]](#), [146](#)

$$\begin{aligned} a_S \text{ from } K_S \rightarrow \pi^0 e^+ e^- &\quad 1.06^{+0.26}_{-0.21} \pm 0.07, \\ a_S \text{ from } K_S \rightarrow \pi^0 \mu^+ \mu^- &\quad 1.54^{+0.40}_{-0.32} \pm 0.06. \end{aligned} \quad (38)$$

With these two numbers, one can constrain the combination  $C_{9+}^{\mu\mu}$  [148](#)  $C_{9+}^{ee}$  via

$$a_S^{\mu\mu} - a_S^{ee} = -\sqrt{2} \operatorname{Re}[V_{td} V_{ts}^* (C_{9+}^{\mu\mu} - C_{9+}^{ee})] = -\sqrt{2} |\lambda_t| (C_{9+}^{\mu\mu} - C_{9+}^{ee}) = 0.5 \pm 0.5. \quad (39) \quad 147$$

A forward-backward asymmetry in these modes could also be used to constrain NP [\[48\]](#), but [150](#)  
there is no experimental information yet. [150](#)

#### 4. $K^+ \rightarrow \pi^+ \mu^+ \mu^-$ [151](#)

Within the SM, this decay is also dominated by LD contributions that arise from an [152](#)  
intermediate-photon state. The LD contributions to these modes are parameterized by the [152](#)  
low-energy constants  $a_+$  and  $b_+$  which are themselves extracted from the measurements [\[53\]](#): [152](#)

$$\begin{aligned} \mathcal{B}_{\text{LD}}^e &= (0.15 - 3.31a_+ - 0.90b_+ + 60.51a_+^2 + 16.36a_+ b_+ + 1.77b_+^2) \times 10^{-8}, \\ \mathcal{B}_{\text{LD}}^\mu &= (1.19 - 19.97a_+ - 6.56b_+ + 120.16a_+^2 + 69.42a_+ b_+ + 10.59b_+^2) \times 10^{-9}. \end{aligned} \quad (40) \quad 153$$

The values of  $a_+$  and  $b_+$  obtained from experiment for the electron mode [\[56\]](#) are [154](#)

$$a_+ = -0.578 \pm 0.016, \quad b_+ = -0.779 \pm 0.066 \quad (41) \quad 155$$

and for the muon mode [57] 156

$$a_+ = -0.575 \pm 0.013, \quad b_+ = -0.722 \pm 0.043. \quad (42) \quad 157$$

We add possible contributions from NP to the branching ratio resulting, for the muon case, in 158

$$\begin{aligned} 10^8 \mathcal{B}(K^+ \rightarrow \pi^+ \mu^+ \mu^-) &= \mathcal{B}_{\text{LD}}^\mu + 9.66 (\lambda_t C_{7+}) + 34 (\lambda_t C_{9+}) + 17.6 (\lambda_t C_{7+})(\lambda_t C_{9+}) \\ &\quad - 48.4 (\lambda_t C_{10+})(\lambda_t C_{P+} \text{ GeV}) + 2.5 (\lambda_t C_{7+})^2 + 31 (\lambda_t C_{9+})^2 \\ &\quad + 74.3 (\lambda_t C_{10+})^2 + 9.46 (\lambda_t C_{P+} \text{ GeV})^2 + 4.34 (\lambda_t C_{S+} \text{ GeV})^2. \end{aligned} \quad (43) \quad 159$$

This has been partially considered in Ref. [40], which provides an expression that includes only 160 the term  $C_{9+}^2$  with a numerical coefficient approximately twice as large as ours.<sup>11</sup> 160

A forward-backward asymmetry can be defined for this mode in terms of the angle  $\theta_{K\mu}$  between 161 the charged-kaon and muon three-momenta in the dilepton center-of-mass frame [58], 161

$$A_{\text{FB}, K^+} = \frac{\mathcal{N}(\cos \theta_{K\mu} > 0) - \mathcal{N}(\cos \theta_{K\mu} < 0)}{\mathcal{N}(\cos \theta_{K\mu} > 0) + \mathcal{N}(\cos \theta_{K\mu} < 0)}. \quad (44) \quad 162$$

In terms of the NP coefficients, the asymmetry is given by<sup>12</sup> 163

$$A_{\text{FB}, K^+} = [0.51 + 0.844 (\lambda_t C_{9+}) + 0.24 (\lambda_t C_{7+})] (\lambda_t C_{S+} \text{ GeV}). \quad (45) \quad 164$$

The latest measurements of these observables produced  $\mathcal{B}(K^+ \rightarrow \pi^+ \mu^+ \mu^-) = (9.17 \pm 0.08) \times 10^{-8}$  165 and  $A_{\text{FB}, K^+} = (0.0 \pm 0.7) \times 10^{-2}$  [57]. 165

Constraints on NP must rely on comparisons between the muon and electron modes and arise 166 from LFU violation (LFUV). One possibility is to take the difference between the branching 166 fraction  $\mathcal{B}(K^+ \rightarrow \pi^+ \mu^+ \mu^-)$  evaluated with  $a_+$  and  $b_+$  extracted from the muon mode, Eq. (41), 166 and with  $a_+$  and  $b_+$  from the electron mode, Eq. (42), 166

$$\Delta \mathcal{B}(K^+ \rightarrow \pi^+ \mu^+ \mu^-) = (-4 \pm 5) \times 10^{-9}, \quad (46) \quad 167$$

and to attribute this difference to the NP terms in Eq. (43). 168

A second possibility is to compare the parameter  $a_+$  as extracted from the muon and electron 169 modes [49, 59]. 169

$$a_+^{\mu\mu} - a_+^{ee} = -\sqrt{2} [V_{td} V_{ts}^* (C_{9+}^{\mu\mu} - C_{9+}^{ee})]. \quad (47) \quad 170$$

With the current values of  $a_+^{\mu\mu, ee}$  [56, 57], this translates into 171

$$a_+^{\mu\mu} - a_+^{ee} = 0.003 \pm 0.021. \quad (48) \quad 172$$

<sup>11</sup> This factor can be traced to an incorrect  $\sqrt{2}$  in the form factor in their Eq. (4.16). 160

<sup>12</sup> Here we differ from [40] in that we normalize the forward-backward asymmetry to a fixed rate, the current 163 experimental value  $\mathcal{B}(K^+ \rightarrow \pi^+ \mu^+ \mu^-) = (9.17 \pm 0.14) \times 10^{-8}$  [17]. 163

## VII. ORGANIZING THE CONSTRAINTS 173

There are ten distinct WCs to describe NP in modes with muons and ten more in modes with electrons if we allow LFUV. Fortunately, as Table VI indicates, many of the modes depend only on one or two WCs, simplifying the numerical study. 174

A direct constraint on  $C_{7,7'}$  can be obtained in principle from radiative hyperon and kaon decays [20, 44, 60]. However, our method to estimate the LD contributions to hyperon decay involves using the  $a$  and  $b$  parameters obtained from experiment, entailing that these could be contaminated by any NP of this form. In principle, a more detailed study of all radiative hyperon modes could be used to isolate any NP here, but we will not pursue it in this paper. Instead, we rely on the constraints obtained from radiative kaon modes by Ref. [44], as listed in Table VII. 177

From Eq. (28) and Tables II-III, one can infer that NP scenarios with  $C_{7,7',9,9',10,10'} \sim 10^4$  and  $C_{P,P',S,S'} \sim 10^5 \text{ GeV}^{-1}$  would be necessary to affect the  $\Sigma^+ \rightarrow p\mu^+\mu^-$  rate at a level that could be observable over the LD contributions. Since this is significantly larger than the bounds placed by kaon physics, we will first impose the kaon restrictions and then use  $\Sigma^+ \rightarrow p\mu^+\mu^-$  to constrain the directions to which the kaons are blind. We will not delve into specific ultraviolet completions in this paper, but simply note that WCs of this order would be consistent with dimensional analysis in models without the CKM suppression  $\lambda_t$  that occurs in the SM and that was rather arbitrarily introduced by the notation of Eq. (25). In Table VI we summarize the WCs that can introduce NP into the different kaon observables discussed thus far. 64

The observables in Table VI are restricted numerically by the 90% confidence-level (CL) bounds (ranges) [17] shown in Table VII, which also displays the corresponding limits for WCs for the cases in which only one of them is constrained. In Eq. (32) we notice that  $K_L \rightarrow \mu^+\mu^-$  restrains a combination of  $C_{10-}$  and  $C_{P-}$ , which we dub  $C_{KL}$ , 179

$$C_{KL} = C_{10-} + \frac{m_{K_0}^2 m_s}{2m_\mu (m_d + m_s)} C_{P-} \simeq C_{10-} + 1.17 \text{ GeV } C_{P-}. \quad (49)$$

180

Observable	WC—linear	WC—quadratic
$\mathcal{B}(K_L \rightarrow \mu^+\mu^-)$	$C_{10-}, C_{P-}$	$C_{10-}, C_{P-}$
$\mathcal{B}(K_S \rightarrow \mu^+\mu^-)$	$C_{S-}$	$C_{S-}$
$\mathcal{B}(K_L \rightarrow \pi^0\mu^+\mu^-)$	$C_{S+}$	$C_{S+}$
$\mathcal{B}(K_L \rightarrow \pi^0e^+e^-)$	$C_{S+}$	$C_{S+}$
$a_S^{\mu\mu} \text{ 178}_{S^*}^{ee}$	$C_{9+}$	—
$a_+^{\mu\mu} \text{ 178}_+^{ee}$	$C_{9+}$	—
$A_{FB,K^+}$	$C_{S+}$	$C_{7+}, C_{9+}, C_{S+}$
$\Delta\mathcal{B}(K^+ \rightarrow \pi^+\mu^+\mu^-)$	$C_{7+}, C_{9+}$	$C_{7+}, C_{9+}, C_{10+}, C_{S+}, C_{P+}$
$\mathcal{B}(\Sigma^+ \rightarrow p\mu^+\mu^-)$	$C_{7\pm}, C_{9\pm}$	$C_{9\pm}, C_{10\pm}, C_{S\pm}, C_{P\pm}$

175

TABLE VI. Wilson coefficients that affect the different kaon and hyperon observables under our scenario of  $CP$ -conserving NP. 176

Observable	90% CL range	constraint on WC
$\mathcal{B}(K_L \rightarrow \mu^+ \mu^-)$ [17]	$(6.66, 7.02) \times 10^{-9}$	$-6.4 \leq C_{KL} \leq -4.7$ or $-1 \leq C_{KL} \leq 0.73$
$\mathcal{B}(K_S \rightarrow \mu^+ \mu^-)$ [61]	$< 2.1 \times 10^{-10}$	$ C_{S-}  < 40 \text{ GeV}^{-1}$
$\mathcal{B}(K_L \rightarrow \pi^0 \mu^+ \mu^-)$ [62]	$< 3.8 \times 10^{-10}$	$ C_{S+}  < 124 \text{ GeV}^{-1}$
$\mathcal{B}(K_L \rightarrow \pi^0 e^+ e^-)$ [63]	$< 2.8 \times 10^{-10}$	$ C_{S+}  < 52 \text{ GeV}^{-1}$
$a_S^{\mu\mu}$ <span style="color:red">+8a_S^{ee}</span>	$(-0.3, 1.3)$	$-603 < C_{9+} < 2611$
$a_L^{\mu\mu}$ <span style="color:red">+8a_{L+}^{ee}</span>	$< 0.035$	$ C_{9+}  < 70$
processes	result from [44]	constraint on WC
$K \rightarrow \pi \pi \gamma$ [44]	$ C_\gamma^-  \lesssim 0.1 G_F m_K$	$ C_{7-}  < 278$
$K \rightarrow \gamma \gamma$ [44]	$ C_\gamma^\pm  \lesssim 0.3 G_F m_K$	$ C_{7\pm}  < 833$

TABLE VII. The 90% CL ranges used for the different modes along with the restrictions they impose on WCs in cases in which only one WC enters the observable.  $C_{KL} \equiv C_{10-} + 1.17 \text{ GeV } C_{P-}$  is the combination constrained by  $K_L \rightarrow \mu^+ \mu^-$ . The bounds in the last two rows are taken from Ref. [44] and are not 90% CL.

Interestingly, this is the same combination that appears in the  $\Sigma^+ \rightarrow p \mu^+ \mu^-$  form-factor in Eq. (27). However, the hyperon mode also depends on  $C_{10-}$  through  $\tilde{F}$  in Eq. (26). The last two rows in Table VII exhibit bounds taken directly from Ref. [44].

After employing all the single parameter bounds from Table VII, we are left with the following constraints:

$$\begin{aligned} -1.2 &\leq 10^8 \Delta \mathcal{B}(K^+ \rightarrow \pi^+ \mu^+ \mu^-) \leq 0.4, \\ |A_{FB,K^+}(K^+ \rightarrow \pi^+ \mu^+ \mu^-)| &\leq 0.12, \\ 0.26 &\leq 10^8 \mathcal{B}(\Sigma^+ \rightarrow p \mu^+ \mu^-) \leq 5.2. \end{aligned} \quad (50)$$

Because the restriction from  $K_L \rightarrow \mu^+ \mu^-$  is found to be much stronger than that from the  $\Sigma^+$  decay, we present the results for  $C_{10-}$  and  $C_{P-}$  in terms of  $C_{KL}$  and its orthogonal counterpart on the  $C_{10-}$ - $C_{P-}$  plane, namely  $C_\Sigma \equiv C_{10-} - 0.85 \text{ GeV } C_{P-}$ . The allowed  $C_{KL}$  range is quoted in Table VII.

Imposing all the constraints simultaneously leads to allowed regions in  $C_{10+}$ - $C_{P+}$  and  $C_\Sigma$ - $C_{9-}$  planes that differ by an order of magnitude. We therefore display them separately in Fig. 6. The  $C_{10+}$ - $C_{P+}$  region is dominantly constrained by  $\Delta \mathcal{B}(K^+ \rightarrow \pi^+ \mu^+ \mu^-)$ , whereas  $\mathcal{B}(\Sigma^+ \rightarrow p \mu^+ \mu^-)$  restricts the parameters  $C_\Sigma$  and  $C_{9-}$ . For the latter, each of the four SM LD solutions leads to slightly different constraints, as illustrated on the right panel of Fig. 6 for the relativistic solutions. The figure shows two-dimensional projections of the full parameter space, but the numerical scan requires all parameters to satisfy all the constraints in Table VII and Eq. (50).

The most important NP contribution to  $\mathcal{B}(\Sigma^+ \rightarrow p \mu^+ \mu^-)$  enters via  $C_{9-}$ , as suggested by the numerical entries in Table II. The allowed range of  $C_{9-}$  corresponding to each of the four relativistic solutions is exhibited on the left panel of Fig. 7. Its right panel displays the correlation between the integrated forward-backward asymmetry and the branching fraction for each of the four solutions.

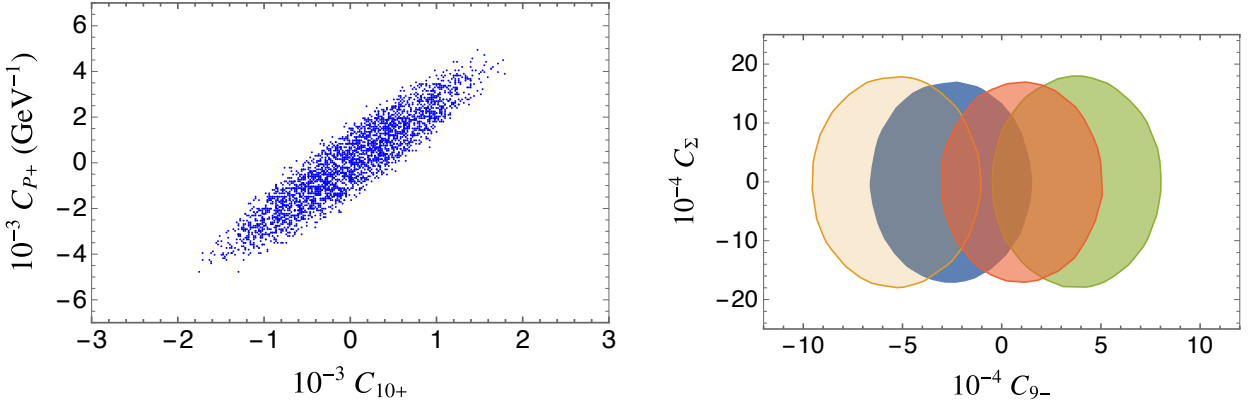


FIG. 6. Left panel: allowed  $C_{10+}$ - $C_{P+}$  parameter space, mostly restricted by  $\Delta\mathcal{B}(K^+ \rightarrow \pi^+\mu^+\mu^-)$ .  
Right panel: allowed  $C_\Sigma$ - $C_{9-}$  parameter space, restricted by the LHCb measurement of  $\mathcal{B}(\Sigma^+ \rightarrow p\mu^+\mu^-)$ . The four relativistic SM LD solutions lead to different allowed regions distinguished by the different colors (blue, yellow, green, red).  
189  
189  
189  
189

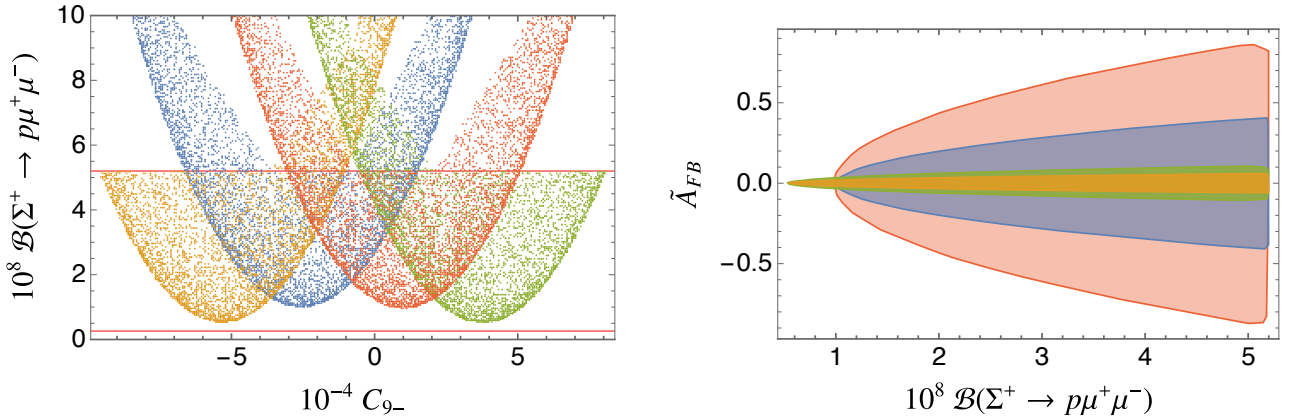


FIG. 7. Left panel: the  $\Sigma^+ \rightarrow p\mu^+\mu^-$  branching fraction as a function of  $C_{9-}$  for each of the four relativistic SM LD solutions (blue, yellow, green, red). Right panel: the corresponding correlation between the branching fraction and the integrated muon forward-backward asymmetry,  $\tilde{A}_{FB}$ , in this decay mode.  
191  
191  
191  
191

The resulting integrated muon forward-backward asymmetry  $\tilde{A}_{FB}$  for  $\Sigma^+ \rightarrow p\mu^+\mu^-$  across the parameter space that survives all the constraints is also most sensitive to  $C_{10-}$ , as can be inferred from Table IV. We show this in the right panel of Fig. 8 for the four relativistic SM LD solutions. The left panel exhibits the correlation between the asymmetry and  $C_{9-}$ , where the variation with  $C_{9-}$  is due to the changing rate. Although Table IV suggests that the asymmetry would be equally sensitive to  $C_{10+}$ , this is not observed in the plots because the allowed range of this parameter is considerably smaller.  
192  
192  
192  
192  
192

It is important to note that the definition we used for  $\tilde{A}_{FB}$  allows for NP in the numerator, but is normalized to the SM rate for each of the four solutions. When the contributions of NP are large this can lead to some misleadingly large anomalies seen in Fig. 8. If we replace the  
195  
195  
195  
195

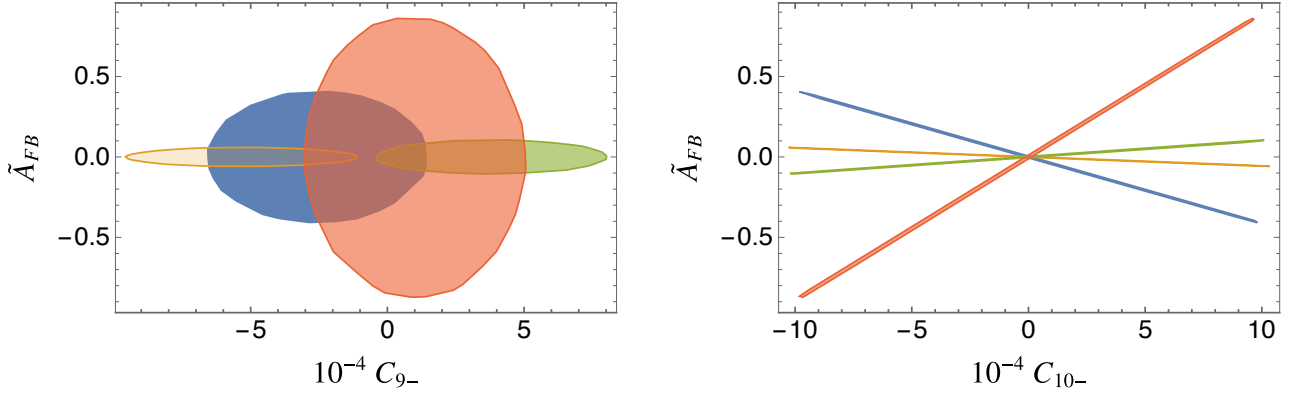


FIG. 8. The region representing the values of  $\tilde{A}_{FB}$  over the allowed range of  $C_{9-}$  (left panel) and  $C_{10-}$  (right panel) for each of the four relativistic SM LD solutions (blue, yellow, green, red).  
193

denominator of the forward-backward asymmetry with the rate including NP contributions, the  
195 anomaly changes to what is exhibited in Fig. 9.  
195

## VIII. SUMMARY AND CONCLUSIONS 196

We have revisited all aspects of the calculation of the rate and muon forward-backward asym-  
197  
metry for the mode  $\Sigma^+ \rightarrow p\mu^+\mu^-$ . This was motivated by the expected more precise measure-  
197  
ment by LHCb as well as recent progress in related modes by BESIII.  
197

Within the SM, we corrected a long-standing issue with the short-distance contribution but  
198 found that it is still negligible with respect to the long-distance contribution. For the latter,  
198 we updated the existing experimental input which reduced the uncertainty in the predictions  
198 that is attributable to experimental error. The fourfold ambiguity in the prediction remains,  
198 but we proposed several ways to address this issue from the experimental side. With the new  
198 numbers, the estimate for hadronic error obtained by interpolating the results from leading-order  
198 relativistic baryon  $\chi$ PT and from its heavy-baryon formulation is also diminished, to the extent  
198 that the four separate solutions remain separate throughout the range.  
198

We then discussed possible constraints on new physics in a model-independent manner through  
199 a general low-energy effective Hamiltonian for  $s \rightarrow d\ell^+\ell^-$  processes. We considered the restric-  
199 tions that can be placed on the different Wilson coefficients from the existing measurements of  
64 rare kaon decays and emphasized the usefulness of the hyperon mode in probing the directions  
199 in parameter space to which the kaons are blind. Aspects of this study exist in the literature,  
199 but this is the first such comprehensive study. Ref. [40], for example, has done a partial study of  
64 the effects of NP on the hyperon mode and the restraints from kaons. Their NP analysis of the  
199 hyperons does not contain all the possible WCs, missing in particular the interference between  
199 SM and NP in the rate which provides the most stringent constraint on  $C_{9-}$ . Within the kaon  
199 modes, we introduced a new observable to constrain NP based on the  $K^+ \rightarrow \pi^+\ell^+\ell^-$  rates.  
199

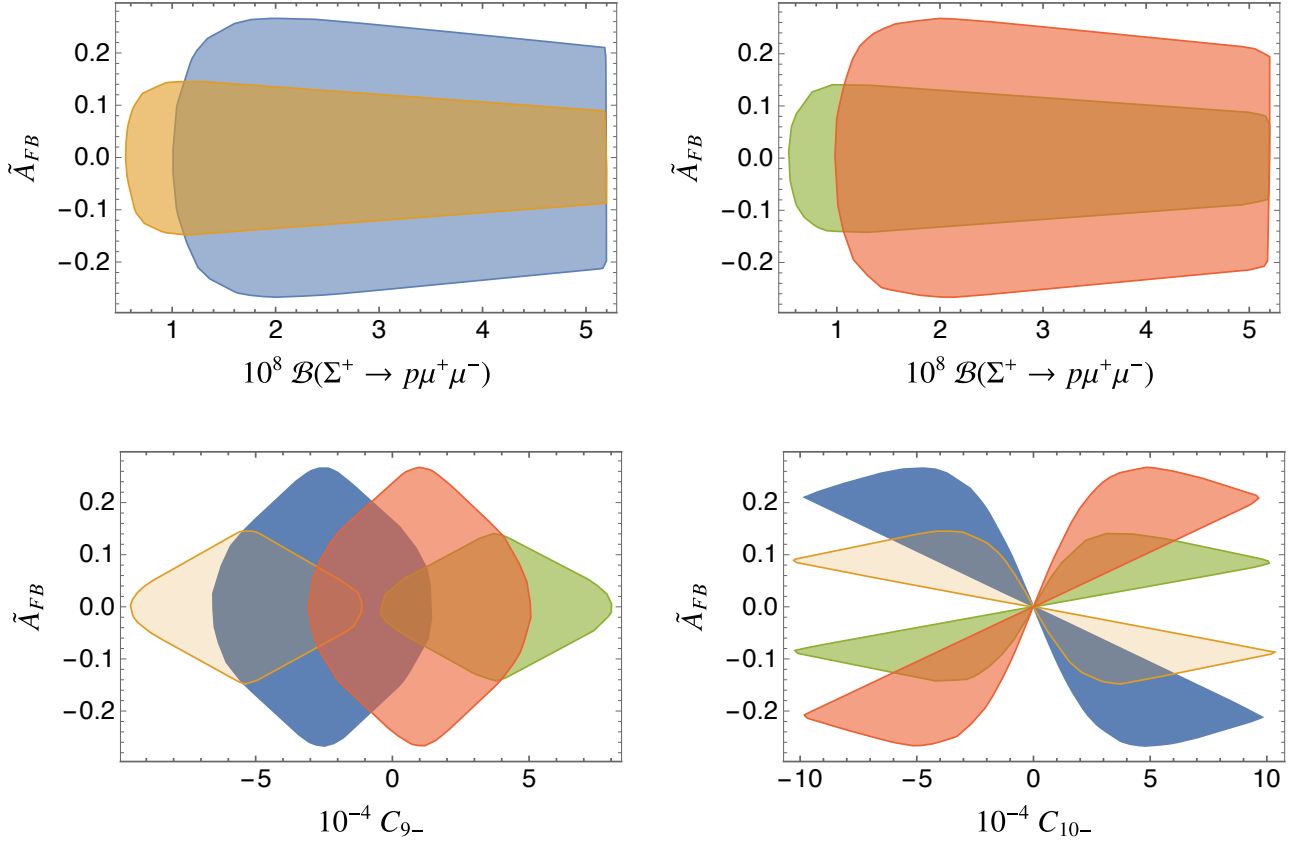


FIG. 9. Upper panels: correlation between the  $\Sigma^+ \rightarrow p\mu^+\mu^-$  branching fraction and integrated muon forward-backward asymmetry,  $\tilde{A}_{FB}$ , when new physics is included in the rate normalizing the latter. Two solutions are plotted on the left panel and two on the right panel, as they overlap. Lower panels: the region representing the values of  $\tilde{A}_{FB}$  over the allowed range of  $C_{9-}$  (left panel) and  $C_{10-}$  (right panel) for each of the four relativistic SM LD solutions (blue, yellow, green, red) when new physics contributions are included in the rate normalizing the forward-backward asymmetry.

## ACKNOWLEDGMENTS

We thank Cong Geng and Hong-Fei Shen for experimental information. The work of A.R. and G.V. was supported in part by an Australian Research Council Discovery Project. We are grateful to F. Mahmoudi for her help with `SuperIso`, which included providing us with her private code for some of the kaon modes discussed in this paper. The work of J.T. was supported in part by the National Key R&D Program of China under Contract No. 2023YFA1606000 and the National Natural Science Foundation of China (NSFC) under Contract No. 11935018. He would like to thank Hai-Bo Li and the Institute of High Energy Physics, Chinese Academy of Sciences, for kind hospitality and support during the preparation of this paper.

- 
- [1] R. Aaij *et al.* (LHCb), Evidence for the rare decay  $\Sigma^+ \rightarrow p\mu^+\mu^-$ , *Phys. Rev. Lett.* **120**, 221803 (2018), arXiv:1712.08606 [hep-ex].
- [2] H.-B. Li, Prospects for rare and forbidden hyperon decays at BESIII, *Front. Phys. (Beijing)* **12**, 121301 (2017), [Erratum: *Front.Phys.(Beijing)* 14, 64001 (2019)], arXiv:1612.01775 [hep-ex].
- [3] A. A. Alves Junior *et al.*, Prospects for measurements with strange hadrons at LHCb, *JHEP* **05**, 203 (2018), arXiv:1808.03477 [hep-ex].
- [4] R. Aaij *et al.* (LHCb), Physics case for an LHCb Upgrade II - Opportunities in flavour physics, and beyond, in the HL-LHC era, (2018), arXiv:1808.08865 [hep-ex].
- [5] A. Cerri *et al.*, Report from Working Group 4: Opportunities in Flavour Physics at the HL-LHC and HE-LHC, *CERN Yellow Rep. Monogr.* **7**, 867 (2019), arXiv:1812.07638 [hep-ph].
- [6] E. Goudzovski *et al.*, New physics searches at kaon and hyperon factories, *Rept. Prog. Phys.* **86**, 016201 (2023), arXiv:2201.07805 [hep-ph].
- [7] G. Anzivino *et al.*, Workshop summary – Kaons@CERN 2023, in *Kaons@CERN 2023* (2023) arXiv:2311.02923 [hep-ph].
- [8] X.-G. He, J. Tandean, and G. Valencia, The decay  $\Sigma^+ \rightarrow p\ell^+\ell^-$  within the standard model, *Phys. Rev. D* **72**, 074003 (2005), arXiv:hep-ph/0506067.
- [9] M. A. Shifman, A. I. Vainshtein, and V. I. Zakharov, On the Weak Radiative Decays (Effects of Strong Interactions at Short Distances), *Phys. Rev. D* **18**, 2583 (1978), [Erratum: *Phys.Rev.D* 19, 2815 (1979)].
- [10] G. Buchalla, A. J. Buras, and M. E. Lautenbacher, Weak decays beyond leading logarithms, *Rev. Mod. Phys.* **68**, 1125 (1996), arXiv:hep-ph/9512380.
- [11] M. Ablikim *et al.* (BESIII), Precision Measurement of the Decay  $\Sigma^+ \rightarrow p\gamma$  in the Process  $J/\psi \rightarrow \Sigma^+\Sigma^-$ , *Phys. Rev. Lett.* **130**, 211901 (2023), arXiv:2302.13568 [hep-ex].
- [12] M. Ablikim *et al.* (BESIII),  $\Sigma^+$  and  $\bar{\Sigma}^-$  Polarization in the  $J/\psi$  and  $\psi(3686)$  Decays, *Phys. Rev. Lett.* **125**, 052004 (2020), arXiv:2004.07701 [hep-ex].
- [13] M. Ablikim *et al.* (BESIII), Test of  $CP$  Symmetry in Hyperon to Neutron Decays, *Phys. Rev. Lett.* **131**, 191802 (2023), arXiv:2304.14655 [hep-ex].
- [14] T. Inami and C. S. Lim, Effects of Superheavy Quarks and Leptons in Low-Energy Weak Processes  $K_L \rightarrow \mu\bar{\mu}$ ,  $K^+ \rightarrow \pi^+\nu\bar{\nu}$  and  $K^0 \leftrightarrow \bar{K}^0$ , *Prog. Theor. Phys.* **65**, 297 (1981), [Erratum: *Prog.Theor.Phys.* 65, 1772 (1981)].
- [15] J. Tandean, Rare hyperon decays with missing energy, *JHEP* **04**, 104, arXiv:1901.10447 [hep-ph].
- [16] N. Cabibbo, E. C. Swallow, and R. Winston, Semileptonic hyperon decays, *Ann. Rev. Nucl. Part. Sci.* **53**, 39 (2003), arXiv:hep-ph/0307298.
- [17] R. L. Workman and Others (Particle Data Group), Review of Particle Physics, *PTEP* **2022**, 083C01 (2022). 5
- [18] S. Neshatpour and F. Mahmoudi, Flavour Physics Phenomenology with SuperIso, *PoS Comp. Tools* **2021**, 010 (2022), arXiv:2207.04956 [hep-ph].
- [19] M. Nielsen, L. A. Barreiro, C. O. Escobar, and R. Rosenfeld, A QCD sum rule approach to the  $s \rightarrow d\gamma$  contribution to the  $\Omega^- \rightarrow \Xi^-\gamma$  radiative decay, *Phys. Rev. D* **53**, 3620 (1996), arXiv:hep-ph/9509297. 24
- [20] J. Tandean, New physics and short distance  $s \rightarrow d\gamma$  transition in  $\Omega^- \rightarrow \Xi^-\gamma$  decay, *Phys. Rev. D* **61**, 114022 (2000), arXiv:hep-ph/9912497.
- [21] J. F. Donoghue, E. Golowich, and B. R. Holstein, *Dynamics of the Standard Model: Second edition* (Cambridge University Press, 2022). 222

- [22] G. Ang *et al.*, Radiative  $\Sigma^\pm$  decays and search for neutral currents, *Z. Phys.* **228**, 151 (1969).
- [23] H. Park *et al.* (HyperCP), Evidence for the Decay  $\Sigma^+ \rightarrow p\mu^+\mu^-$ , *Phys. Rev. Lett.* **94**, 021801 (2005), arXiv:hep-ex/0501014.
- [24] R. E. Behrends, Photon Decay of Hyperons, *Phys. Rev.* **111**, 1691 (1958).
- [25] I. V. Lyagin and E. K. Ginzburg, On  $\Sigma^+ \rightarrow pe^+e^-$  and  $\Sigma^+ \rightarrow p\mu^+\mu^-$  Decays, *Sov. Phys. JETP* **14**, 653 (1962).
- [26] L. Bergstrom, R. Safadi, and P. Singer, Phenomenology of  $\Sigma^+ \rightarrow p\ell^+\ell^-$  and the structure of the weak non-leptonic Hamiltonian, *Z. Phys. C* **37**, 281 (1988).
- [27] L. K. Gershwin, M. Alston-Garnjost, R. O. Bangerter, A. Barbaro-Galtieri, T. S. Mast, F. T. Solmitz, and R. D. Tripp, Asymmetry parameter and branching ratio of  $\Sigma^+ \rightarrow p\gamma$ , *Phys. Rev.* **188**, 2077 (1969).
- [28] A. Manz, S. Reucroft, R. Settles, G. Wolf, J. Marraffino, C. Roos, J. Waters, and M. Webster, A new measurement of  $\Sigma^+ \rightarrow p\gamma$  decay properties, *Phys. Lett. B* **96**, 217 (1980).
- [29] M. Kobayashi, J. Haba, T. Homma, H. Kawai, K. Miyake, T. S. Nakamura, N. Sasao, and Y. Sugimoto, New measurement of the asymmetry parameter for the  $\Sigma^+ \rightarrow p\gamma$  decay, *Phys. Rev. Lett.* **59**, 868 (1987). 238  
112
- [30] M. Foucher *et al.* (E761), Measurement of the asymmetry parameter in the hyperon radiative decay  $\Sigma^+ \rightarrow p\gamma$ , *Phys. Rev. Lett.* **68**, 3004 (1992).
- [31] R. Aaij *et al.* (LHCb), Measurement of the photon polarization in  $\Lambda_b^0 \rightarrow \Lambda\gamma$  decays, *Phys. Rev. D* **105**, L051104 (2022), arXiv:2111.10194 [hep-ex].
- [32] R. O. Bangerter, *Nonleptonic decay of Sigma hyperons*, Ph.D. thesis, Calif. U. Berkeley (1969).
- [33] F. Harris, O. E. Overseth, L. Pondrom, and E. Dettmann, Proton Polarization in  $\Sigma^+ \rightarrow p\pi^0$ , *Phys. Rev. Lett.* **24**, 165 (1970).
- [34] E. H. Bellamy *et al.*, Polarisation in the reaction  $\pi^+p \rightarrow K^+\Sigma^+$  at 1.11 GeV/c, *Phys. Lett. B* **39**, 299 (1972). 203
- [35] N. H. Lipman *et al.*, A test of the  $\Delta I = 1/2$  rule and the Lee-Sugawara relation in the decay  $\Sigma^+ \rightarrow p\pi^0$ , *Phys. Lett. B* **43**, 89 (1973). 236
- [36] F. Erben, V. Gülpers, M. T. Hansen, R. Hodgson, and A. Portelli, Prospects for a lattice calculation of the rare decay  $\Sigma^+ \rightarrow p\ell^+\ell^-$ , *JHEP* **04**, 108, arXiv:2209.15460 [hep-lat]. 24
- [37] F. Erben, V. Gülpers, M. T. Hansen, R. Hodgson, and A. Portelli, Progress on the exploratory calculation of the rare Hyperon decay  $\Sigma^+ \rightarrow p\ell^+\ell^-$ , *PoS LATTICE2022*, 315 (2023), arXiv:2212.09595 [hep-lat]. 238  
238  
238
- [38] X.-G. He, J. Tandean, and G. Valencia, Decay rate and asymmetries of  $\Sigma^+ \rightarrow p\mu^+\mu^-$ , *JHEP* **10**, 040, arXiv:1806.08350 [hep-ph]. 61  
239
- [39] R. Aaij *et al.* (LHCb), Differential branching fraction and angular analysis of  $\Lambda_b^0 \rightarrow \Lambda\mu^+\mu^-$  decays, *JHEP* **06**, 115, [Erratum: *JHEP* 09, 145 (2018)], arXiv:1503.07138 [hep-ex].
- [40] L.-S. Geng, J. M. Camalich, and R.-X. Shi, New physics in  $s \rightarrow d$  semileptonic transitions: rare hyperon vs. kaon decays, *JHEP* **02**, 178, arXiv:2112.11979 [hep-ph].
- [41] G. Isidori, C. Smith, and R. Unterdorfer, The rare decay  $K_L \rightarrow \pi^0\mu^+\mu^-$  within the SM, *Eur. Phys. J. C* **36**, 57 (2004), arXiv:hep-ph/0404127. 203
- [42] F. Mahmoudi, SuperIso v3.0, flavor physics observables calculations: Extension to NMSSM, *Comput. Phys. Commun.* **180**, 1718 (2009). 243
- [43] S. Neshatpour and F. Mahmoudi, Flavour Physics with SuperIso, *PoS TOOLS2020*, 036 (2021), arXiv:2105.03428 [hep-ph]. 165  
244
- [44] P. Mertens and C. Smith, The  $s \rightarrow d\gamma$  decay in and beyond the Standard Model, *JHEP* **08**, 069, 5 arXiv:1103.5992 [hep-ph]. 245

- [45] V. Chobanova, G. D'Ambrosio, T. Kitahara, M. Lucio Martinez, D. Martinez Santos, I. S. Fernandez, and K. Yamamoto, Probing SUSY effects in  $K_S^0 \rightarrow \mu^+ \mu^-$ , *JHEP* **05**, 024, arXiv:1711.11030 [hep-ph]. 246
- [46] M. Gorbahn and U. Haisch, Charm Quark Contribution to  $K_L \rightarrow \mu^+ \mu^-$  at Next-to-Next-to-Leading Order, *Phys. Rev. Lett.* **97**, 122002 (2006), arXiv:hep-ph/0605203.
- [47] G. Buchalla, G. D'Ambrosio, and G. Isidori, Extracting short distance physics from  $K_{L,S} \rightarrow \pi^0 e^+ e^-$  decays, *Nucl. Phys. B* **672**, 387 (2003), arXiv:hep-ph/0308008.
- [48] F. Mescia, C. Smith, and S. Trine,  $K_L \rightarrow \pi^0 e^+ e^-$  and  $K_L \rightarrow \pi^0 \mu^+ \mu^-$ : a binary star on the stage of flavor physics, *JHEP* **08**, 088, arXiv:hep-ph/0606081.
- [49] G. D'Ambrosio, A. M. Iyer, F. Mahmoudi, and S. Neshatpour, Anatomy of kaon decays and prospects for lepton flavour universality violation, *JHEP* **09**, 148, arXiv:2206.14748 [hep-ph].
- [50] G. Ecker, A. Pich, and E. de Rafael,  $K \rightarrow \pi \ell^+ \ell^-$  decays in the effective chiral lagrangian of the standard model, *Nucl. Phys. B* **291**, 692 (1987).
- [51] G. D'Ambrosio, G. Ecker, G. Isidori, and J. Portoles, The decays  $K \rightarrow \pi \ell^+ \ell^-$  beyond leading order in the chiral expansion, *JHEP* **08**, 004, arXiv:hep-ph/9808289.
- [52] G. D'Ambrosio, D. Greynat, and M. Knecht, On the amplitudes for the CP-conserving  $K^\pm(K_S) \rightarrow \pi^\pm(\pi^0)\ell^+\ell^-$  rare decay modes, *JHEP* **02**, 049, arXiv:1812.00735 [hep-ph].
- [53] V. Cirigliano, G. Ecker, H. Neufeld, A. Pich, and J. Portoles, Kaon Decays in the Standard Model, *Rev. Mod. Phys.* **84**, 399 (2012), arXiv:1107.6001 [hep-ph].
- [54] J. R. Batley *et al.* (NA48/1), Observation of the rare decay  $K_S \rightarrow \pi^0 e^+ e^-$ , *Phys. Lett. B* **576**, 43 (2003), arXiv:hep-ex/0309075 [hep-ex].
- [55] J. R. Batley *et al.* (NA48/1), Observation of the rare decay  $K_S \rightarrow \pi^0 \mu^+ \mu^-$ , *Phys. Lett. B* **599**, 197 (2004), arXiv:hep-ex/0409011 [hep-ex].
- [56] J. R. Batley *et al.* (NA48/2), Precise measurement of the  $K^\pm \rightarrow \pi^\pm e^+ e^-$  decay, *Phys. Lett. B* **677**, 246 (2009), arXiv:0903.3130 [hep-ex].
- [57] E. Cortina Gil *et al.* (NA62), A measurement of the  $K^+ \rightarrow \pi^+ \mu^+ \mu^-$  decay, *JHEP* **11**, 011, [Addendum: *JHEP* 06, 040 (2023)], arXiv:2209.05076 [hep-ex].
- [58] C.-H. Chen, C. Q. Geng, and I.-L. Ho, Forward backward asymmetry in  $K^+ \rightarrow \pi^+ l^+ l^-$ , *Phys. Rev. D* **67**, 074029 (2003), arXiv:hep-ph/0302207. 246
- [59] A. Crivellin, G. D'Ambrosio, M. Hoferichter, and L. C. Tunstall, Violation of lepton flavor and lepton flavor universality in rare kaon decays, *Phys. Rev. D* **93**, 074038 (2016), arXiv:1601.009701.166 260 [hep-ph]. 260
- [60] X.-G. He and G. Valencia, Constraints on  $s \rightarrow d\gamma$  from radiative hyperon and kaon decays, *Phys. Rev. D* **61**, 075003 (2000), arXiv:hep-ph/9908298.
- [61] R. Aaij *et al.* (LHCb), Constraints on the  $K_S^0 \rightarrow \mu^+ \mu^-$  Branching Fraction, *Phys. Rev. Lett.* **125**, 231801 (2020), arXiv:2001.10354 [hep-ex].
- [62] A. Alavi-Harati *et al.* (KTeV), Search for the Decay  $K_L \rightarrow \pi^0 \mu^+ \mu^-$ , *Phys. Rev. Lett.* **84**, 5279 (2000), arXiv:hep-ex/0001006 [hep-ex].
- [63] A. Alavi-Harati *et al.* (KTeV), Search for the Rare Decay  $K_L \rightarrow \pi^0 e^+ e^-$ , *Phys. Rev. Lett.* **93**, 021805 (2004), arXiv:hep-ex/0309072 [hep-ex]. 264